Advanced Biomanufacturing of Neural Organoids from Human Pluripotent Stem Cells

By

Seyyed Alireza Aghayeemeibody

A dissertation submitted in partial fulfillment

of the requirements for the degree of

Doctor of Philosophy

(Materials Science and Engineering)

at the

UNIVERSITY OF WISCONSIN-MADISON

2021

Date of oral examination: 03/11/2020

The dissertation is approved by the following members of the Final Oral Committee:

Randolph S. Ashton, Professor, Biomedical Engineering

Kristen Masters, Professor, Biomedical Engineering

Sean Palecek, Professor, Chemical and Biological Engineering

Li-Sheng Turng, Professor, Mechanical Engineering

Krishanu Saha, Professor, Biomedical Engineering

Table of Contents

Abstract

Organoids derived from human pluripotent stem cells (hPSCs) have become widely explored in vitro for tissue modeling and developmental studies. Neurally differentiating hPSCs possess the ability to result in formation of polarized areas of neural stem cells (NSCs), known as neural rosettes, which resemble cross-sectional slices of the embryonic neural tube and develop into neural organoids. Current neural organoid derivation protocols mainly rely on spontaneous self-organization of cell aggregates that occurs within 3D spheroids and provide minimal control throughout their formation. This yields neural organoids containing microscale biomimetic cytoarchitectures. However, at the macroscale and as a whole tissue, these organoids commonly develop abnormal morphologies and lack a consistent cellular composition. The current lack of control over in vitro organoid morphogenesis at the micro- to macroscale is a major factor that limits reproducibly of anatomically correct tissues and their ability to serve as optimal in vitro models. Overall, this prevents researchers from using organoid technology at its maximum potential.

Here, we have developed a platform and methodology for engineering arrays of microscale neural tissues with biomimetic neural tube morphology and the ability to further expand into neural organoids from different regions of brain and spinal cord. Frist, we use soft lithography and robotic microcontact patterning (R-μCP) to manufacture substrates that are sequentially micropatterned with polymer brushes and further functionalized with various chemistries and peptides. We determined that R-μCP can be deployed to manufacture biocompatible substrates with consistent surface uniformity, sequential patterning precision of ±15-20 μm, and can enable spatiotemporal control over neural organoid morphology.

Next, we describe a protocol to bioengineer hPSC-derived NSC tissues with controlled induction of a biomimetic singular rosette cytoarchitecture. Control of the NSC aggregates morphology is provided using R-μCP substrates. Variables such as biochemical factors (e.g., growth factors, signaling inhibition molecules) as well as biophysical parameters (e.g., geometry, hPSCs surface density) were found to be critical for singular rosette induction. The resulting arrays of singular rosette tissues model the cytoarchitecture of a transverse slice of the embryonic neural tube. The Ashton lab previously found that circular patterns of 250 μm diameter could generate forebrain neuroepithelial tissues with cytoarchitectures that are biomimetic to in vivo neural tube slices as characterized by the single polarized expression of N-Cadherin and early neural progenitor marker Pax6. To our knowledge, this is the closest demonstration of a neural tube mimetic in vitro, and it can be the first step into standardizing the formation of neural organoids.

Finally, this platform was used to radially expand arrays of spatially isolated, singular forebrain neural rosettes on R-μCP culture substrates. R-μCP substrates were modified in situ to induce radial outgrowth of the rosettes to produce large neural tissue slices. Here, we investigate how temporal changes in substrate biochemistry can be used to control maintenance and proliferation of neural rosettes during their radial outgrowth phase to eventually generate cell phenotypes and morphologies characteristic of human neural tissues. We synthesized and immobilized a variety of potential cell binding molecules on R-μCP substrates to determine which combination are optimal for recapitulating neural tissues expansion and generating uniform neural organoids. We found that a clickable RGD peptide sequence can be used at different concentrations to modify the R-μCP substrates in situ and provide tissue expansion within contained outgrowth areas.

The long-term goal is to eventually use this platform to biomanufacture developmentally relevant neural organoids as tissue slices from different regions of central nervous system. Interfacing this

platform with induced pluripotent stem cells (iPSCs) and techniques for hPSC gene-editing and patient-specific cellular reprogramming could allow for advanced study of neurodegenerative disease mechanisms and open the door for potentially novel high throughput drug and toxin screening methods. Ultimately, the work presented here will lay the foundation for facilitating a greater understanding of neurogenesis and future neurodegenerative disease prevention and treatment.

Acknowledgements

I would first like to thank God for the priceless life I have been given and all the strength and perseverance I have been gifted. I will use these blessings in a way that impacts the society and people all around the world to live a better life.

I cannot be any more proud and grateful for being a part of the University of Wisconsin-Madison, Department of Materials Science & Engineering, Biomedical Engineering, and the city of Madison as a whole. The past few years have been the best and most life-changing years of my life. I am beyond happy with all of the great experiences I had in my time here.

I want to first and foremost thank the Ashton lab for welcoming me as a Graduate Student. I have grown a lot from working in the Ashton lab and all the people I worked with. This has made my experience enjoyable. I am grateful for all the trainings, collaborations, and priceless times I have had with members in the lab.

I also want to thank all of the people I have had the opportunity to collaborate with from other labs. I would like to thank Dr. Saha for involving me in the gene editing platform collaboration project and providing a valuable opportunity for me to learn new skills. Dr. Jose A. Rodriguez-Martinez and Prof. Aseem Ansari for a valuable connection we made over the collaboration project and valuable training and feedback I received from them.

I would like to acknowledge all of the funding that has supported me during my time at UW-Madison. First, I would like to thank the Chemistry Department for a teaching assistantship I was provided over a year that helped me to continue on my education. I would like to thank Biomedical Engineering Department for hosting me as teaching assistant for two semesters in their program. I would also like to mention the research grants awarded to my PI that have

supported my research such as NSF, the EPA, the Burroughs Welcome Fund, the Stem Cell and Regenerative Medicine Center (SCRMC), and the National Institute for Neurological Disorders. I would like to thank the Wisconsin Institute for Discovery (WID) for providing the home for my research experience. It has been amazing to work in such a collaborative workspace and I truly appreciate everyone that has made my time in the WID so great.

I would also like to thank my friends in Madison who helped me to keep a balanced lifestyle and made my journey so enjoyable. Thanks to Gavin Knight, Nisha Iyer, Maria Estevez, Katherine Jeffris, Brady Lundin, Jason McNulty, Jared Carlson–Stevermer, Benjamin Steyer, Amr Abdeen and Nicole Piscopo for the valuable times I spent with them in the lab environment and lab activities. I truly enjoyed a good friendship I developed with Carlos Marti Figueroa and Brett Napiwocki, who provided many fun times playing in Pool Leagues together. I would like to also thank my friends in the Madison community for making Madison feel so comfortable for me as an international student. You have all become family to me and I will always be grateful for the wonderful experience we had throughout our time here.

I would also like to thank my family who supported me throughout the years. In particular, I would first like to thank my mother and sister. Next, I would like to thank my schizophrenic brother who motivated me to learn more about his problem and better understand science behind it. I would hope my work along with other researchers' limitless efforts can better serve patients with neurodegenerative diseases.

I would also like to thank all my committee members, Prof. Kristen Masters, Professor Sean Palecek, Prof. Tom Turng and Prof. Krishanu Saha for the feedback and support during my preliminary exam and towards the final stages of my dissertation.

Finally, I would like to thank my PI and Mentor, Dr. Randolph Ashton. Thank you for the opportunity to join your lab as a graduate student. Thank you for your guidance not only as a research mentor but also as a career and life mentor. I will always be grateful for your feedback in my research project and support in my career path.

Chapter 1: Introduction and background

1. Human Embryonic Stem Cells

Embryonic stem cells are defined by their ability to renew themselves, meaning that they are able to perform mitotic divisions to maintain their population (pluripotency), and also their ability to differentiate into different cell phenotypes [1]. Due to these two important features, stem cells have many potential applications in basic biological studies and therapeutic and clinical research. In developing embryos, human embryonic stem cells can differentiate into all cell types of the main germ layers, i.e., ectoderm, endoderm, and mesoderm [2]. The resulting cells can participate in the regeneration and replacement of renewable organs such as blood, skin and digestive tissues [3].

2. Human Induced Pluripotent Stem Cells

In 2006, Japanese researchers reported the production of a new type of powerful stem cells that can evade the immunological problem of embryonic stem cells because they can be derived from the donor's own cells. They are called Induced pluripototent stem cells (iPSCs) and are produced by the viral expression of four important precursor genes in somatic cells. iPSCs have all the capabilities of embryonic stem cells, including the ability to produce a complete organism, and have all the potential uses of embryonic stem cells, including precise disease modeling, high throughput toxin and drug screening, and extensive clinical translations [4].

3. Central Nervous System (CNS) Cell Phenotypes

Human neural cells and clinical transplants were initially isolated from fetal tissue sources [5]. This approach has been universally replaced by the more sustainable human pluripotent stem cell (hPSC, i.e.,hESC and iPSC) source. Neural stem cells (NSC) derivation protocols have advanced to highly efficient differentiation methods using hPSC monolayers in the absence of transforming growth factor-beta (TGF-β) and bone morphogenetic protein (BMP) pathway activity [6,7]. This in vitro NSC phenotype is remarkably identical to its in vivo counterpart, and enables scientists to generate numerous neuronal and glial phenotypes through direct implementation of developmental biology principles. Using iPSCs, patient-specific central nervous stem (CNS) cells can also be generated for disease modeling and further practical applications in regenerative cell therapy (Figure 1) [8].

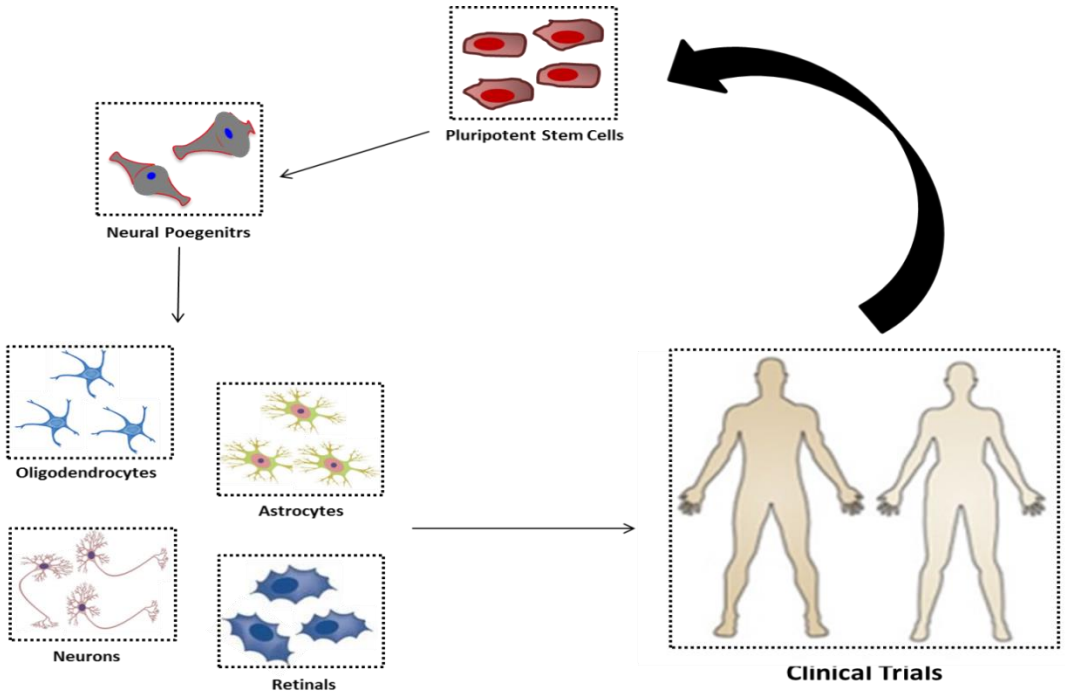

Figure 1: Neural cells derivation from human pluripotent stem cells.

4. Neural Organoids

Aggregates of NSCs in 2D and 3D cultures exhibit a self-organization that yields biomimetic CNS tissue structures. Neural organoids initiate with areas known as “neural rosettes” that recapitulate early stage morphogenic processes of the neural tube before developing into neural tissues with unique cellular and cytoarchitectural structures. Neural organoids have been used widely to model aspects of human central nervous system development, neurogenesis and neuropathology in settings previously infeasible for model organism (Figure 2) [9].

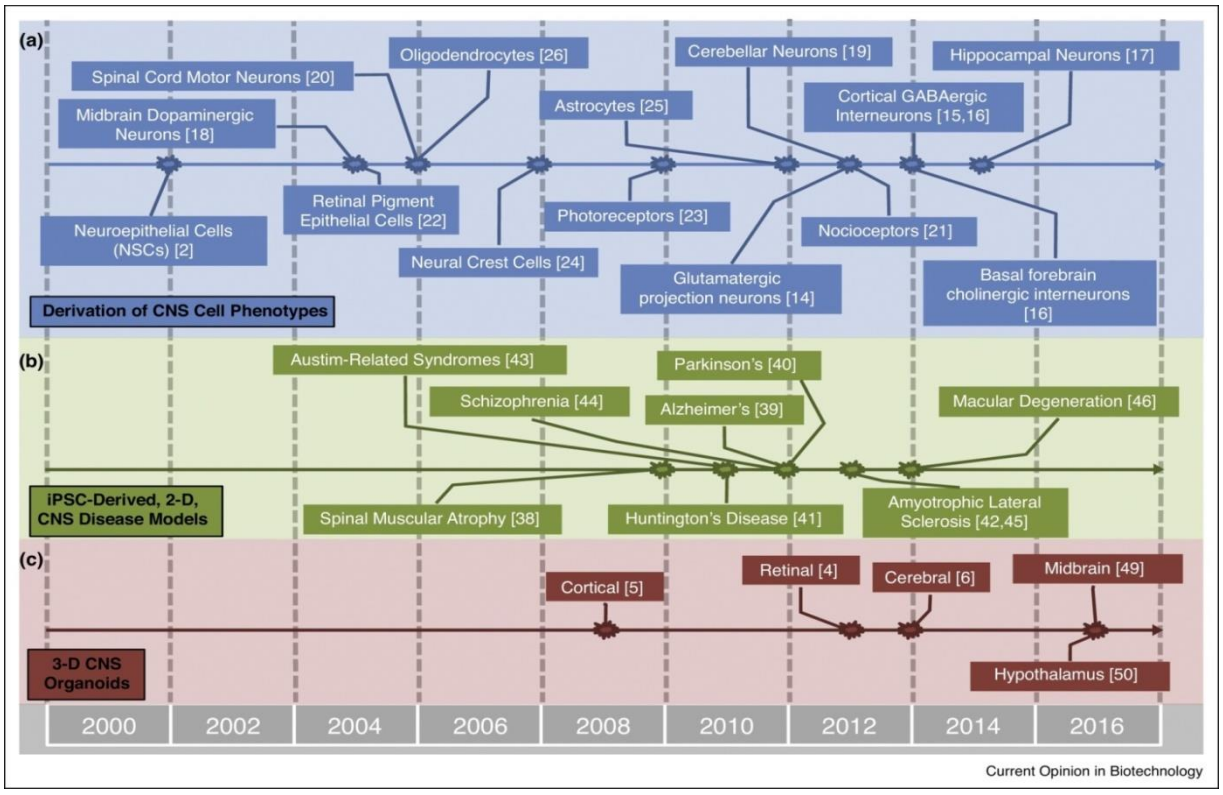

Figure 2: Chronology of progress in deriving CNS cells and tissues. Timeline list seminal studies describing derivation of human CNS (a) regional cell phenotypes, (b) 2-D disease-in-a-dish models, and (c) 3-D organoids from hPSCs. Includes references cited in the review; it is not a comprehensive list [9].

In vivo the neural tube serves as the primordial tissue progenitor for all primary neuronal and glial cells of the developing CNS and is morphologically characterized by a single layer of columnar neuroepithelial cells exhibiting apical polarization of N-cadherin and basal deposition of a basal lamina (Figure. 3) [10].

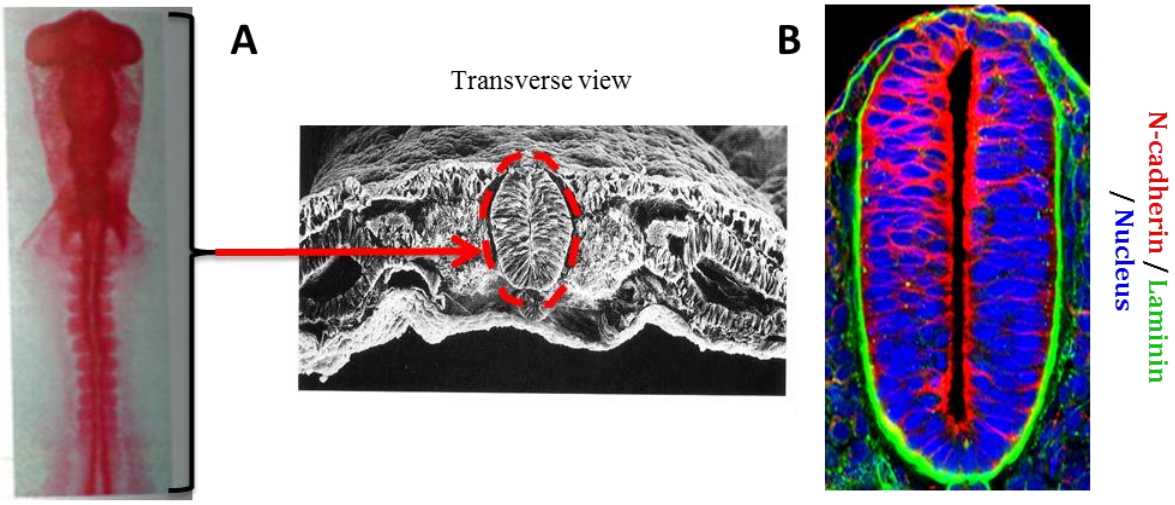

Figure 3: A) Chick Embryo (HH10) neural tube in the embryo [10]. B) Cross-section of chick neural tube, 50 µm scale bar. (By Gwenval LeDreau et al. Instituto de Biología Molecular de Barcelona-CSIC).

The neural tube then expands radially via simultaneous differentiation and migration of neuroepithelial progenitors. Neuroeptihelial cells remain at the apical boundary of the tissue undergoing a cell division phenomenon unique to the neural tube, known as interkinetic nuclear migration (IKNM) [11]. The mechanics of these cell divisions, and subsequent radial expansion of the tissue, vary depending on the location along the neural tube's rostrocaudal (R/C) axis [12].

5. Corticogenesis

Generation of neural organoids in vitro requires careful recapitulation of complex developmental processes that occur in vivo. In forebrain regions of the neural tube, neuroepithelial cells differentiate into radial glial cells that maintain cell-cell interactions at the apical surface while extending processes to the readily expanding basal boundary [13]. Radial glial cells are maintained as a pool of neural progenitors throughout embryonic development. A balance of cell-cell and cell-extracellular matrix (ECM) interactions is considered crucial for facilitating forebrain development into the classic stratified cerebral cortical structure [14].

The cerebral cortex is characterized by six distinct layers of neurons. This laminated structure is produced by the birth of post-mitotic neurons in successive waves throughout the course of corticogenesis following a highly organized radial migration program [15]. During early corticogenesis, dividing cells occupy the ventricular zone (VZ), and a thin layer of cortical primordium forms the pre-plate [16]. Then the first group of neurons exiting the cell-division cycle migrates out of the ventricular zone and navigates into a sub-ventricular zone (SVZ) and eventually forms a cortical plate region exhibiting initial cortical neurons [17]. Therefore, the cortex is assembled in an 'inside-out' manner, such that early-born neurons reside in deeper layers and later-born neurons in more superficial layer (Figure 4). Cortical organoids developed from hPSCs and iPSCs are very powerful platforms for biological studies and provide researchers priceless information [18].

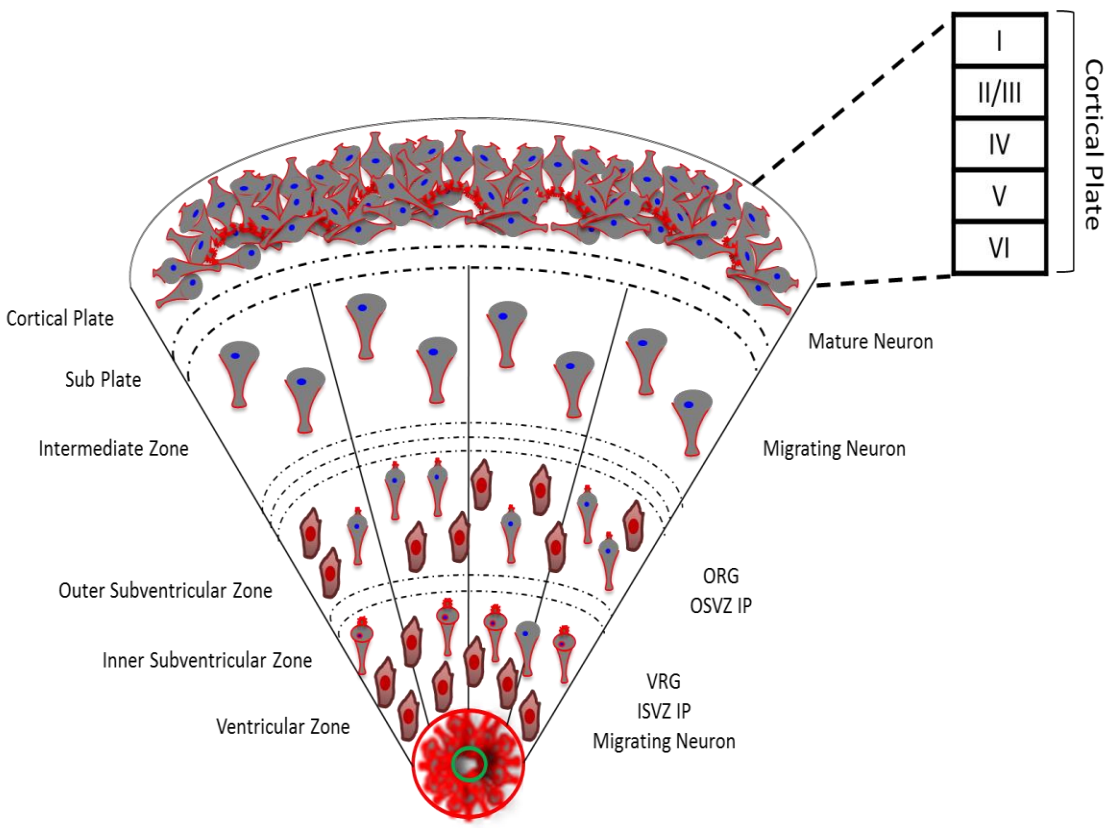

Figure 4: Anatomical organization of corticogenesis and interkinetic nuclear migration (IKNM) for laminated structure of corticogenesis.

There have been high quality studies to develop protocols to facilitate neural organoid technologies and improve on the current limitations. The reproducibility of neural organoid anatomy is necessary to use organoids to replace animal models in clinical translation and discovery of new drugs and treatments for neurological disorders. Chemically undefined culture conditions and lack of reproducible macroscale cytoarchitectural features remain the biggest challenge to standardization of neural organoid derivation protocols. Current published protocols for generation of cerebral organoids with similar regional diversity and cortical differentiation can be adapted with chemically defined substrates to facilitate morphology consistency and reproducibility limitations [19].

6. Engineering cell culture substrates

In tissue engineering, material-cell interactions are of great importance and play a significant role in cells behaviors. To precisely control and model these interactions, biomimetic culture substrates have been developed that contain the spatial heterogeneity of microenvironmental cues observed within *in vivo* tissues. Long chain alkanethiols can spontaneously bind to gold coated surfaces. The long alkyl chain of these molecules forms an ordered close-packed monolayer with balancing of Van der Waals forces between adjacent carbon chains. This well-ordered and closely packed monolayer forms a new surface interface with properties being defined on the molecular scale based on the end group functionality of alkanethiols present in the monolayer [20] (Figure 5). Self-assembled monolayers (SAMs) of alkanethiols on gold substrates can be used to create surfaces at which the cell-surface interface can be defined and be used to engineer substrates that can control stem cell adhesion and provide further ligands immobilization. These substrates can be used to investigate how cellular microenvironments can affect stem cell fate in culture systems [21]. Many techniques and studies have been performed on developing SAMs substrates for various biological applications despite their short time durability and modification difficulties. Factors such as the alkanethiols chain length, surface density and the solvent defines the chemical composition of the resulting SAMs substrates [22].

6.1 Polymer Brushes

In order to improve stability of SAMs substrates, by preventing oxidization of the sulfur-gold coordination bond, polymer brushes have been developed. Polymer brushes are very thin polymer coatings that are made up of polymer chains that are covalently connected to the substrate. Polymer chains are so densely packed together that they have to be fully stretched and

perpendicular to the surface to prevent overlapping with other chains. This change in conformity and density create new properties in polymer brushes and make them suitable for long term biological applications by improving their stability under culture conditions [23]. The "grafting from" method for synthesizing polymer brushes involves starting polymerization from the surface and is broadly used for biological applications. The alkanethiol initiator SAMs are first placed on the surface of the substrate (which can be flat or a particle), then the surface is exposed to a solution of a monomer and, if necessary, a catalyst. Ideally, polymerization should only be done on the surface and no reaction should occur in the solution. With the advancement of polymerization methods, it is possible to control the thickness of the brush, the distribution of the molecular mass and the percentage composition of the chain components, as well as the copolymer brushes [24]. A variety of polymerization methods, such as cationic, anionic, radically controlled polymerization, and ring-forming polymerization have been used to synthesize "grafting from" polymer brushes. Atom transfer radical polymerization (ATRP), a controlled radical polymerization method, has been used more than other methods in biological applications due to the wide range of usable monomers, compatibility with organic and aquatic environments, and lower cytotoxicity for cell culture applications (Figure 5) [25].

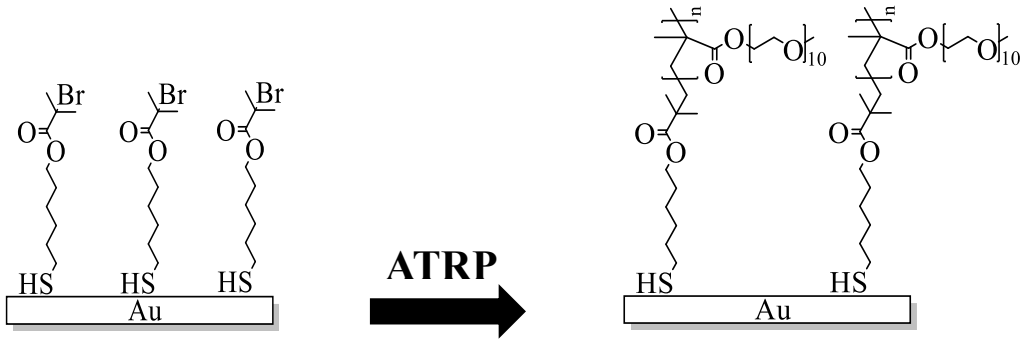

Figure 5: Schematic of SAMs and their transition into polymer brushes via atomic transfer radical polymerization.

6.2 Soft Lithography

Soft lithography is an inexpensive, fast and simple technique that has been developed to create complex chemical patterns on substrates. Using this technique alkanethiol initiator SAMs can be micropatterned (µP) on gold surfaces and further be used to create µP polymer brushes synthesis on substrates (Figure 6). Micropatterned polymer brushes with reactive end groups can be further reacted with bioactive small molecules and peptides to control cell adhesion and final tissue morphology [26]. The engineered micropatterned substrates using polymer brushes is a powerful platform for defining and controlling cell-biomimetic surface interactions and generating complex tissues [27-28].

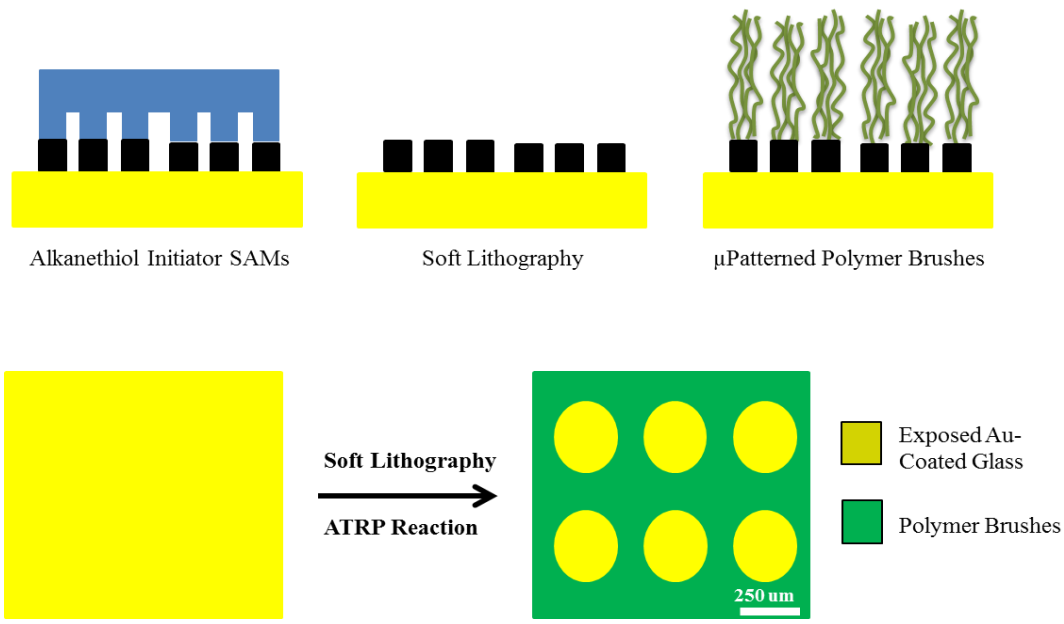

Figure 6: Schematic of soft lithography technique to pattern substrates with SAMs and generate polymer brushes on micropatterned regions on surface.

Poly(ethylene glycol) (PEG) brushes have already been widely used as bio-inert polymers to develop culture substrates with microscale regions. These PEG-grafted substrates can further be modified with covalently immobilized ligands and provide bio-specific interactions [29]. Micropatterned click-functionalized PEG brushes can be used to develop a variety of cellular microenvironments that enable biospecific interactions between immobilized ligands and stem cells. The Ashton lab has previously developed 2D micropatterned substrates to engineer the morphology of neurally differentiating hPSC tissues within geometric confined areas and regulate neural rosette emergence [30]. They have discovered that circular micropatterns of 200 – 250 μm diameter (0.031 – 0.049 mm2) were observed to most effectively induce singular neural rosette emergence within forebrain neuroepithelial tissues at 80 – 85% efficiency when initially seeded as hPSCs [31]. During the rosette induction period, the hPSCs morphed from a 2D monolayer and into 3D multi-layered and neurally differentiated cellular tissues with cytoarchitectures mimetic of the early neural tube. In this thesis, robotic microcontact printed substrates were used sequential graph micropattered PEG brushes on gold-coated coverslips to create a culture platform capable of transforming hPSC-derived, singularly polarized neural rosette tissues into organotypic CNS tissue slices. This was accomplished by developing surface chemistry protocols to modify the surface in situ allowing radial expansion of neural rosette tissue from their initial micropatterned confinements. Neuronal differentiation can occur at the expanding tissues' periphery while maintaining a singular neuroepithelial rosette as the morphogenesis center. Reproducible and high throughput induction expansion of this biomimetic morphological cytoarchitecture is a pre-requisite for advanced biomanufacturing of human CNS organoids with consistent biomimetic anatomy.

Chapter 2: Design and Manufacture of Micropatterned Culture Substrates for Controlled Radial Tissue Outgrowth

1. Introduction

Microenvironmental interactions play a significant role in stem cell fate and behavior. There has been continuous work by researchers and scientists to develop platforms to precisely control the stem cell microenvironment. Microcontact printing (μCP) is a soft lithography technique that has been used for various applications including spatially patterning surfaces that can be further modified for biological applications. In this technique, an elastomeric stamp of polydimethylsiloxane (PDMS) presenting nano to microscale features is coated with a deposition material (e.g., solution of alkanethiols) and then patterned on substrates (e.g., gold coted surface) by conformal contact [30,31].

While μCP is a versatile technique for patterning large surface areas with features as small as 10 nm, it remains a challenge to efficiently align multiple patterns onto a single substrate with high accuracy and precision while simultaneously providing maximal flexibility in substrate modification chemistry. The Ashton lab has previously developed a robotic μCP (R-μCP) method using a vision guided, selectively compliant articulated robotic arm (SCARA) that eliminates these limitations and performs sequential patterning within 15-20 μm precision. The R-μCP method allows maximum flexibility in substrate fabrication and PDMS stamp design, and it permits convenient exchange of PDMS stamps. Further, the Ashton lab demonstrated that R-μCP can be used to sequentially pattern a single substrate with 2 different stamps while maintaining an accuracy and precision of <20 μm in the X and Y directions and <0.5° in θ even with periodic removal of the substrate from the system between stamping [32].

In bioengineering, it is very important to be able to provide spatiotemporal control of tissue morphology and cell fate at the micron scale. Culture substrates presenting grafted poly(ethylene glycol) (PEG) brushes can be used to create microscale, non-fouling and bio-inert regions, and can also be further treated with variety of chemistries including click chemistry to immobilize bio-specific tethered ligands onto grafted PEG brushes. Orthogonally functionalized, R-μCP, PEG-grafted culture substrates can be an ideal platform for controlling tissue morphology and growth in vitro. These substrates can be used as a practical system for investigating the roles of bioactive ligands on hPSC fate and migration [33].

Micropatterned substrates have been used to bioengineering neural organoids. For example, the Ashton lab has already used soft lithography techniques to develop micropatterned substrates that when seeded with hPSCs and neurally differentiated can induce, with >80% reproducibility, the emergence of singularly-polarized neural rosette tissues, which are in vitro analogs of the neural tube's neuroepithelium. This demonstrates that control over the initial microscale morphology of hPSC or NSC aggregates in 2D culture is critical for effective control of subsequent rosette morphogenesis [31].

In this chapter, I use the technology developed in the Ashton lab to design and develop multifunctional micropatterned substrates capable of generating single neural rosettes and regulating their radial tissue outgrowth. The chemistry techniques described here provide a robust method for manufacturing culture substrates that can facilitate rational and reproducible production of organotypic tissue structures in vitro. I further evaluate the uniformity and consistency in manufacturing of the substrates, and I analyze the accuracy and precision of the

sequential patterns developed by R-μCP. Lastly, I seed hPSCs directly onto the R-μCP substrates and assess their biocompatibility and micropatterning fidelity.

2. Materials and Methods

2.1 Materials

Type 1 glass microscope coverslips (Fisher Scientific), Copper(II) bromide (99.999% trace metals basis), 2,2′-bipyridine (BiPy; ≥99%), N,N,N′,N″,N″ pentamethyldiethylenetriamine (PMDETA, 99%), L-ascorbic acid, oligo(ethylene glycol) methyl ether methacrylate (OEGMA, Mn = 450), sodium azide, triethylamine (Et3N, ≥99%), copper(II) sulfate (CuSO4, ≥99%), tris[(1-benzyl-1H-1,2,3-triazol-4- yl)methyl]amine (97%), propargylamine (98%), donkey serum, methanol (for HPLC ≥99%), N,N-dimethylformamide (DMF, anhydrous, 99.8%), dimethyl sulfoxide (DMSO, anhydrous, ≥99.9%) were purchased from Sigma-Aldrich (Milwaukee, WI). Streptavidin-Alexa Fluor 488 conjugate, Streptavidin-Alexa Fluor 546 conjugate, and Dulbecco's phosphate-buffered saline (DPBS) were purchased from Life Technologies. OEGMA monomer was purified with basic Al_2O_3 column to remove the inhibitor. The alkanethiol initiator ω-mercaptoundecyl bromoisobutyrate was purchased from Prochimia Inc. Azide-PEG4-biotin, acetylene-PEG4-biotin, and DBCO-PEG4-biotin conjugates were purchased from Click Chemistry Tools. H9 (WA09) human embryonic stem cells (hESCs) were provided from WiCell. Gibco™ Essential 8™ Medium, Gibco™ Essential 6™ Medium, DMEM/F-12 Medium, Tissue-culture polystyrene (TCPS) were purchased from ThermoFisher. All other materials and reagents not labeled with a source denotation were purchased from Fisher and used as received.

2.2 Generation of Robotic Micropatterned (R-μCP) Culture Substrates

2.2.1 Gold Coating Substrates

Type 1 18x18 mm glass microscope coverslips were cleaned by sequential immersion in toluene and methanol followed by sonication for 1 min in acetone and were completely dried using a nitrogen gas stream. Using a CHA-600 Metal Evaporator (Telemark) 35 Å of titanium followed by 180 Å of gold were deposited onto the coverslips. Gold-coated coverslips were then rinsed 3 times with absolute ethanol.

2.2.2 PDMS Stamps Design and Preparation

To create micropatterned silicon masters for generating PDMS stamps, AutoCAD software was used to design the photomask's feature patterns. The micropattern design of arrays of annului, with 250 μm inner and 300 μm diameter outer circles, was created as post stamps. A second micropattern design of arrays of 800 μm circles was also designed as a well stamp. Final photomask designs were sent to FlowJEM Inc. for silicon wafer manufacture. To make elastomeric stamps for soft lithography, poly(dimethyl siloxane) (PDMS; Slygard 184 Kit) mixture was prepared according to manufacturer instructions, i.e., a 10:1mixture of PDMS and curing agent. The mixture was poured on top of the micropatterned silicon wafers and was cured overnight at 60 °C. The cured PDMS elastomer was then carefully peeled from the silicon wafer surface and a straight edge razor was used to trim excess cured elastomer from the PDMS stamp.

2.2.3 Robotic Microcontact Printing and Generation of Annulus Outgrowth Features

Using robotic microcontact printing technology, ω-mercaptoundecyl bromoisobutyrate in absolute ethanol solution (2 mM) was patterned on gold-coated surfaces as a SAM using PDMS

post stamps. Micropatterned substrates were then put in schlenk reaction flasks separately and were sealed and degassed by vacuum. SAMs were further used in a surface-initiated ATRP reaction to graft poly(ethylene glycol) methacrylate (PEGMA) brushes from the surface. ATRP reaction solution was prepared by dissolving (8 g, 16.7 mmol) of oligo (ethylene glycol) methyl ether methacrylate (OEGMA, Mn = 475) in water (7.5 ml) and methanol (7.5 ml) and adding copper(II) bromide (0.08 mmol, 17.9 mg), and 2′,2-bipyridine (0.24 mmol, 37.5 mg) to the solution. 5ml of a ATRP reaction solution was injected into each reaction flask. To start the reactions, 500 µl of L-sodium ascorbate solution in ultra-pure water (400 mM) was injected into each reaction flask. A solution color change was observed at this time (Figure 1). Thin Film Measurement System Filmetrics F20 (Reflectometer) was used to measure the thickness of transparent micropatterned PEGMA brushes.

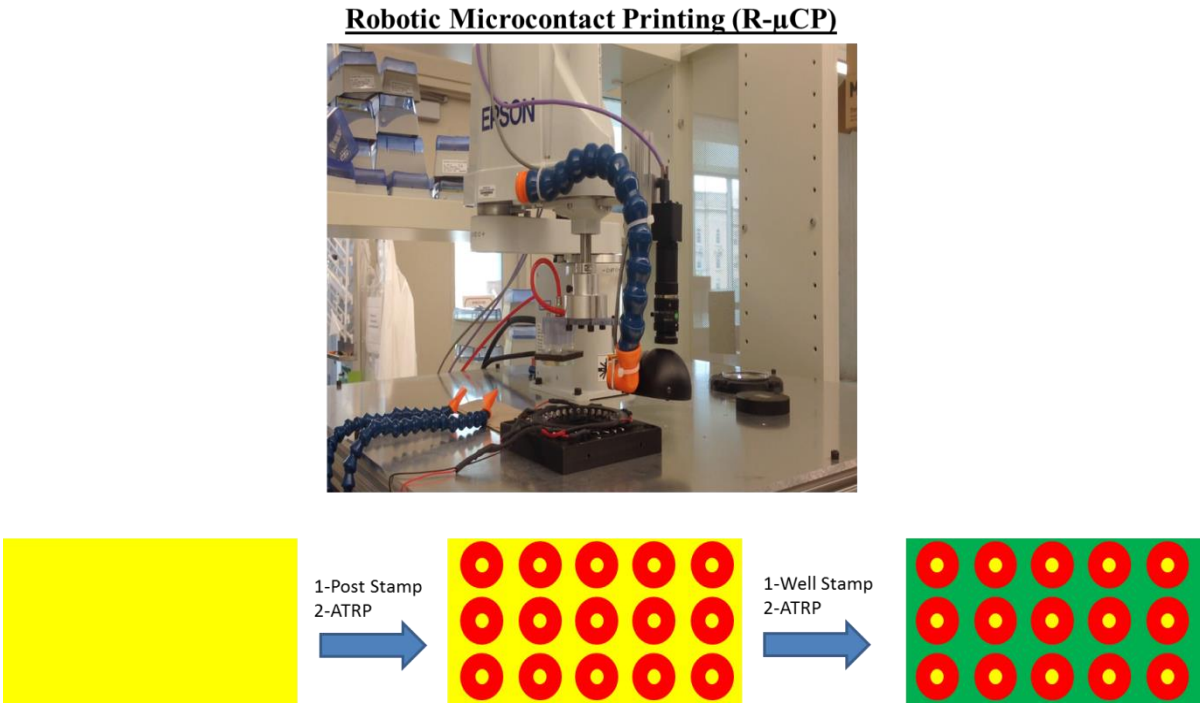

Figure 1: Schematic of robotic microcontact printing process to graft PEGMA brushes with heterogeneous functionalities on gold coated substrates.

2.2.4 Modification of PEGMA Brushes with Azide Functional Groups

To visualize the patterns of (PEGMA) brushes, we functionalized the features with azide groups. Azide substitution was performed by reacting micropatterned PEGMA brushes in 0.1 M sodium azide solution in DMF at room temperature with 1 hour reaction time. This was followed by rinsing with water and ethanol and substrates were fully dried with nitrogen.

2.2.5 Robotic Microcontact Printing and Backfilling with un-modified PEGMA Brushes

Robotic microcantact printing was performed as previously described above in section 2.2.3. This time the PDMS stamp with 800μm diameter circles was used to cover and backfill outside the previously micropatterned annulus PEGMA features with alkanthiol initiators. SAMs were further used for surface initiated ATRP reaction with PEGMA as previously described.

2.2.6 Surface Modification of Backfilled PEGMA Brushes with Acetylene Groups

Nucleophilic substitution by propargylamine was performed by reacting micropatterned PEGMA brushes in 0.1 M propargylamine in DMSO solution at room temperature for 2 hours reaction time. This was followed by rinsing with water and ethanol and substrates were fully dried with nitrogen.

2.2.7 Surface Conjugation of Azide Functional Groups with DBCO-PEG4-Biotin

R-μCP substrates functionalized with azide groups were put in a 6 well polystyrene dish and were rinsed 5 times with DBPS. 2 ml of DBPS containing 20 μM DBCO-PEG4-Biotin was added to each well and incubated for 24 hr at RT. R-μCP substrates were rinsed again 5 times with DPBS upon completion.

2.2.8 Immunofluorescent Detection of Biotinylated Azide Groups

Biotin conjugates were detected by immunostaining using streptavidin-Alexa Fluor 546 conjugates. Substrates were covered in 3% donkey serum/DPBS and shaken for 1 h to block nonspecific binding. After aspiration of the blocking solution, 20 μL of streptavidin-Alexa Fluor 546 conjugate (2 mg/mL) in 3% donkey serum/DPBS was added and the slides were shaken for 2 h at room temperature. Then the substrates were washed with Tris-buffered saline (TBS, pH 7.4) twice for 5 min each. A confocal fluorescence microscope was used to image R-μCP substrates.

2.2.9 Surface Conjugation of Acetylene Functional Groups with Azide-PEG4-Biotin

R-μCP substrates functionalized with Acetylene groups were placed in a 20 ml glass reaction vial. 6 ml of a 1:1 v/v water/DMF solution containing copper sulfate (15 mM), Tris[(1-benzyl-1H-1,2,3-triazol-4-yl)methyl]amine (TBTA, 30 mM) and 562μM azide-PEG4-Biotin conjugate were added to each glass reaction vial. 1 ml of L-ascorbic acid (0.15 mM) in water was added to the mixture to initialize the reaction which proceeded for 8 h at room temperature. After completion substrates were washed thoroughly with water and ethanol, and were dried using nitrogen. Light was avoided during the entire time of reaction.

2.2.10 Immunofluorescent Detection of Biotinylated Acetylene Groups

R-μCP substrates were blocked in DPBS (3% Donkey Serum) for 1 hr at RT. Biotinylated acetylene groups were stained with Streptavidin-488 conjugate (2 μg/ml) in DBPS (3% Donkey Serum in PBS) for 2 hr at room temperature. Substrates were rinsed 5 times with DPBS for 10 min afterward. A confocal fluorescence microscope was used to image R-μCP substrates.

2.3 Cell Seeding and Culture

R-μCP substrates were coated by 1 mg Matrigel in 12 mL of DMEM/F12 media for 12 hours, and were then seeded with hPSCs (passages 30-40) at 100K cells per cm^2 density. The cells were cultured on the micropatterned substrates for 3-7 days in E6 media. Brightfield microscopy was used for imaging.

3. Results and Dissection

3.1 Manufacturing of R-μCP Substrates

Robotic microcontact printing was used to design and develop micropatterned substrates capable of presenting orthogonal functional groups on a single surface. Robust surface chemistry techniques are described for manufacturing of rational and reproducible micropatterned culture substrates [29,30]. As shown in Figure 2A, azide functional groups were conjugated to PEGMA brushes via nucleophilic substitution. DBCO-PEG4-Biotin can be further reacted with azide groups through a click chemistry reaction. Streptavidin-546 fluorescent conjugates were added to label biotin molecules for confocal microscopy imaging (Figure 2B).

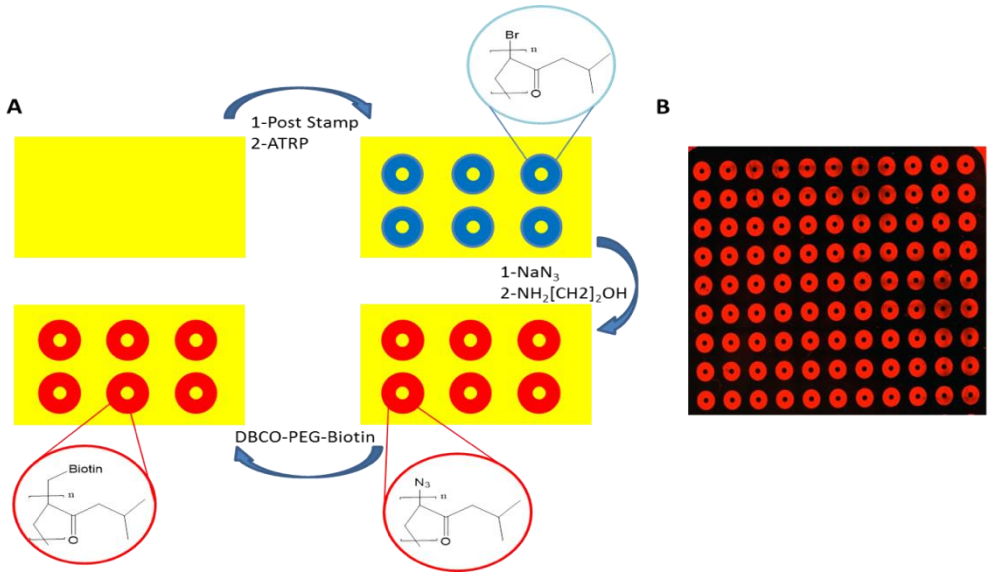

Figure 2: A) Schematic of R-μCP of PEGMA brushes, azide functionalization and DBCO-PEG4-Biotin conjugation. B) Confocal image of streptavidin-546 fluorescent labeled biotin molecules conjugated substrates.

A second robotic printing was then performed using well stamps and the same procedure was followed for grafting (PEGMA) brushes. This time brushes were functionalized with acetylene groups by using propargylamine (Figure 3A). Azide-PEG4-Biotin were reacted with conjugated acetylene groups through a click chemistry reaction and labeled with Streptavidin-488 for fluorescent visualization of orthogonal micropatterned brush patterns.

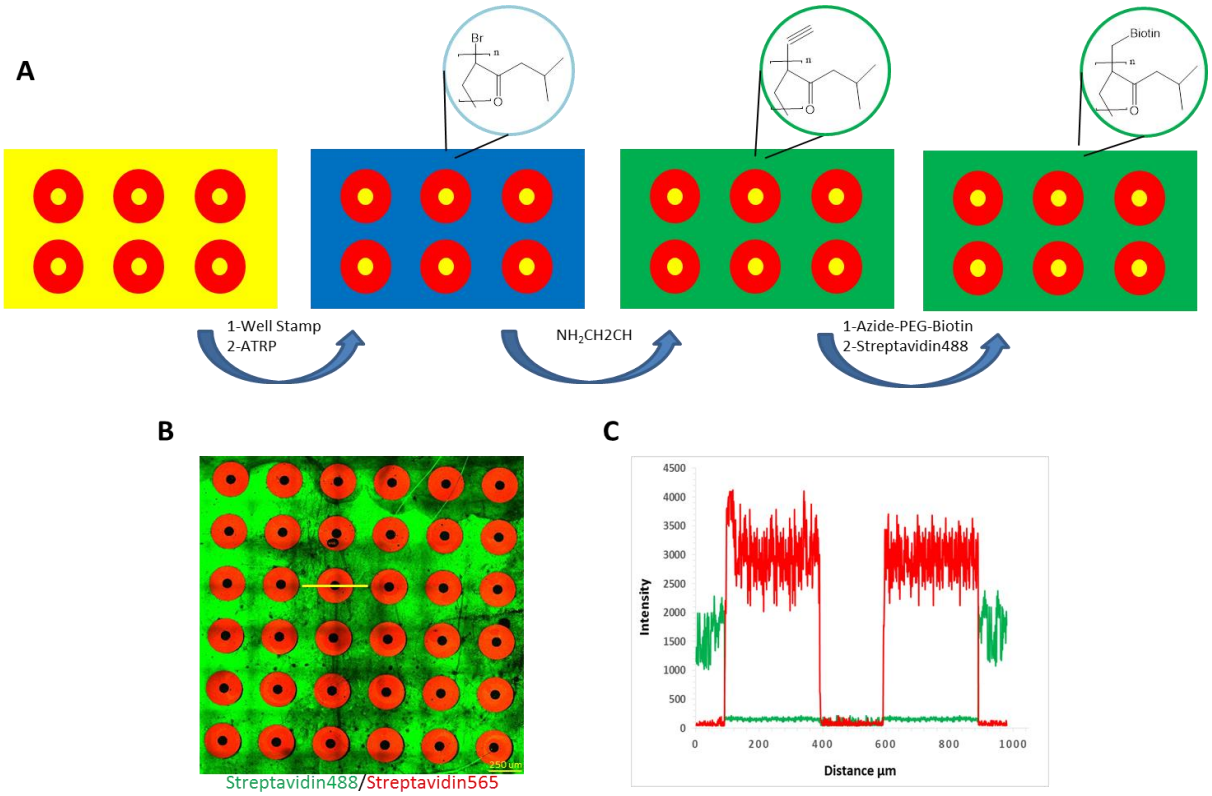

Figure 3: A) Schematic of sequential R-µCP of PEGMA brushes, acetylene functionalization and Azide-PEG4-Biotin conjugation. B) Confocal images of streptavidin-488 and streptavidin-546 fluorescent labeled biotin molecules conjugated substrates. C) Fluorescent intensity profile of streptavidin-488 and -546 labled substrates across the yellow line scan.

3.2 Estimated Robotic Microcontact Printing Accuracies

Upon sequential patterning and orthogonal functionalization of PEGMA brushes on substrates, Streptavidin-546 and -488 fluorescently labeled images were generated separately using confocal microscopy. Nikon software was used to generate (X,Y) data points for corners of each fluorescently labeled image and a custom MATLAB program was developed to perform fast image analysis and quantify offsets of the sequential patterns and estimate robotic microcontact printing accuracies (Appendix 2). R-μCP can be used to sequentially pattern a single substrate with 2 different stamps while maintaining an accuracy and precision of 15 ±5μm in the X and Y directions and 0.1˚±.05˚ in θ even with periodic removal of the substrate from the system between stamping (Figure 4).

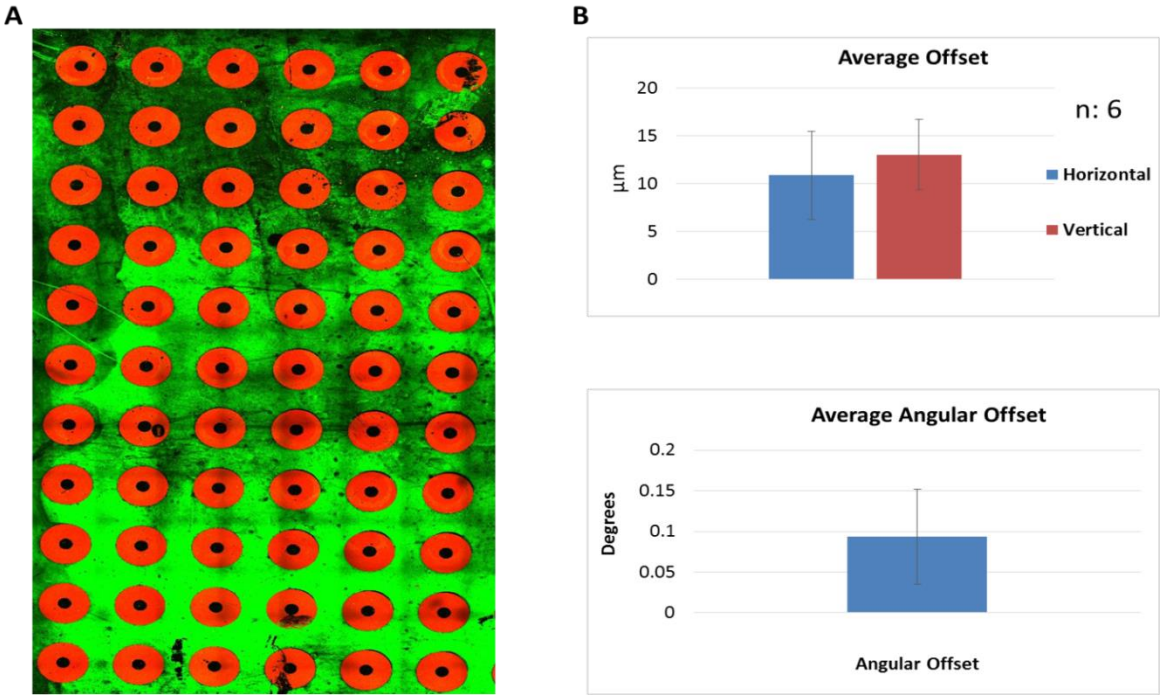

Figure 4: A) Confocal images of sequentially micropatterned substrates and labeled with Streptavidin-546 and Streptavidin-488 fluorescent conjugates. B) Estimated robotic microcontact printing offset accuracies. A MATLAB program was developed to analyze X, Y, and angular (θ) errors for 50 features on 6 different substrates.

3.3 Uniformity Analysis of R-µCP Culture Substrates

In order to execute a uniform radial tissue expansion, patterns of PEGMA brushes with consistent and uniform thickness and functionalization are required. Here, confocal microscopy fluorescent intensity measurements were used to evaluate the uniformity of the Streptavidin-546 fluorescent conjugation throughout patterned regions. This can be used as an indicator to demonstrate how uniform potential peptide conjugates could be presented on micropatterned PEGMA brushes. First, a standard curve equation was derived to correlate fluorescent intensity of the patterns to the Streptavidin-546 surface density (ng/µm2) (Appendix 1). To create a standard curve for surface density quantification, 0.5 mL droplets from known concentrations of Streptavidin-546 solution were dried on top of a gold coated substrate. The integrated fluorescence intensity per area was calculated using confocal microscopy. This correlation was then used to assess substrate to substrate uniformity and was also used to quantify the uniformity of the patterns within each substrate and inside each pattern (Figure 5). R-µCP substrates pose a consistent surface uniformity throughout multiple replicates and can provide uniform patterns within each substrate with no statistical difference across replicate micropatterned surfaces.

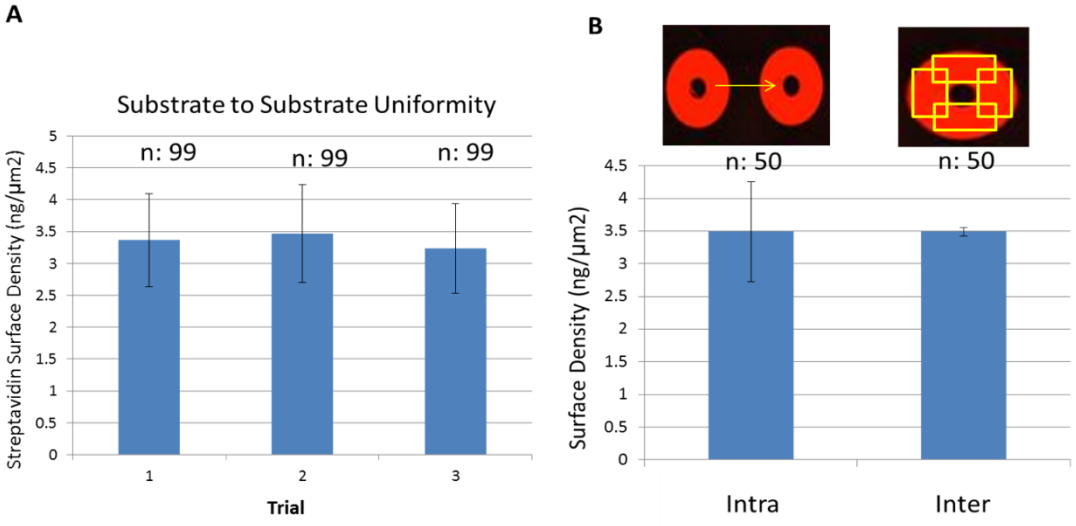

Figure 5: A) Substrate to substrate surface uniformity. B) Feature to feature uniformity within each substrate.

Nikon Software was used to develop graphs of fluorescent intensity of Streptavidin-546 conjugated R-μCP substrates across micropatterned substrate (Figure 6A). Fluorescence intensity profile is used to evaluate surface uniformity throughout the surface. A thickness surface profiler was used to measure the thickness of PEGMA brushes inside micropatterned features and a consistent thickness of 180 nm of polymer thin film was recorded (Figure 6B).

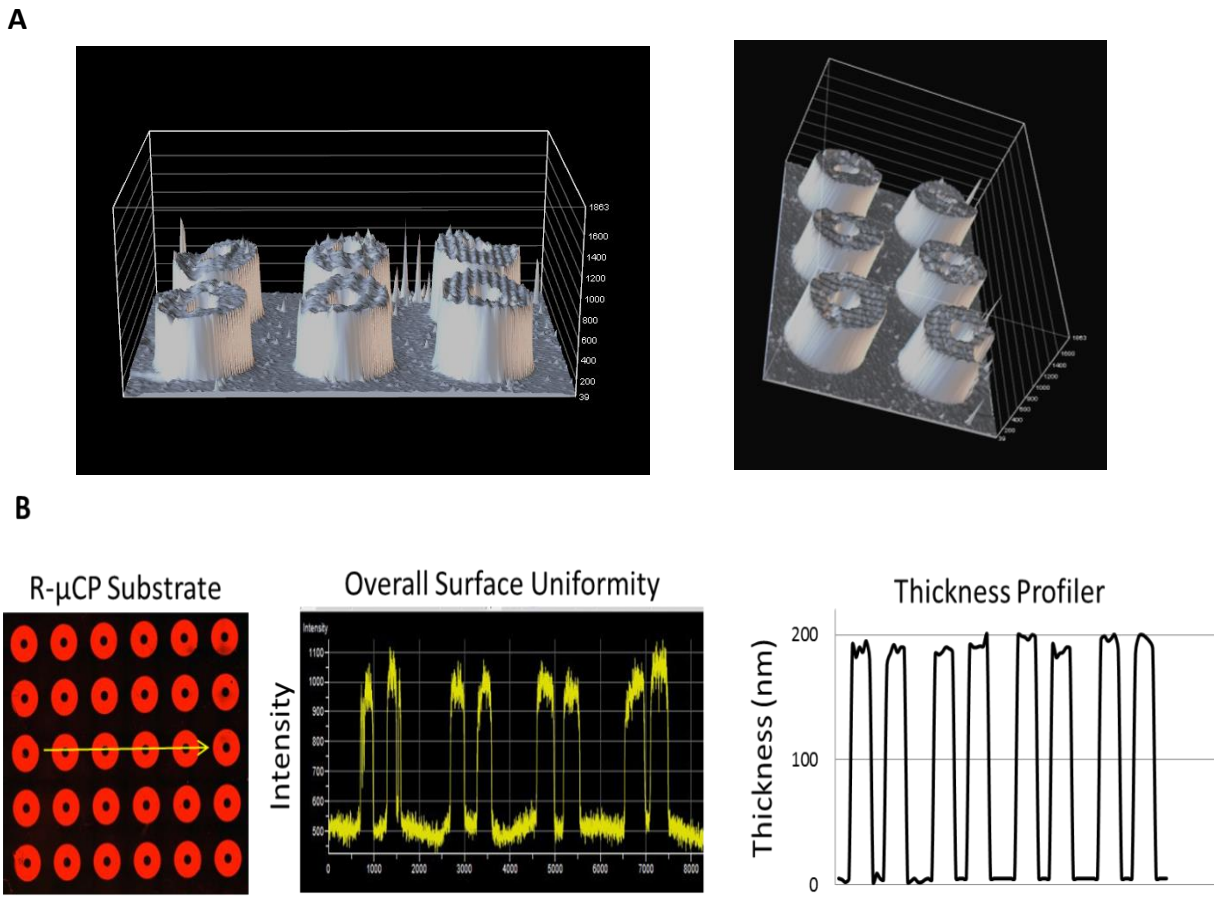

Figure 6: A) Nikon 3D images of PEGMA brushes labeled with Streptavidin-546 fluorescent conjugates. B) Confocal images of PEGMA brushes labeled Streptavidin-546 with a line scan of fluorescent intensity measurement and thickness profiler over the yellow arrow.

3.4 Functionalization of PEGMA Brushes on R-μCP Substrates at Different Densities

It is important to be able to modify the micropatterned surfaces with different densities of cell adhesive ligands. Bromoacetic acid is used to convert hydroxyl groups to bromides on (PEGMA) brushes side chains [29]. These bromide groups are then replaced by azides that are subsequently conjugated with biotin molecules. The less biotin molecules presented on the surface then less Streptavidin-546 can be further conjugated to the substrate. Therefore, a correlation between mmoles of the DBCO-PEG4-Biotin and Streptavidin-546 surface density (ng/μm^2) was generated to confirm this matter and evaluate the achievable range of conjugation surface density on R-μCP substrates (Figure 7A). DBCO-PEG4-Biotin conjugated onto micropatterned polymer brushes at different mmole rates showed statistically significant different surface densities of streptavidin-546 fluorescent conjugation. Streptavidin-546 surface density (ng/μm^2) was quantified as previously described, and a decrease in surface density was observed on R-μCP substrates conjugated with DBCO-PEG4-Biotin at lower mmoles (Figure 7B).

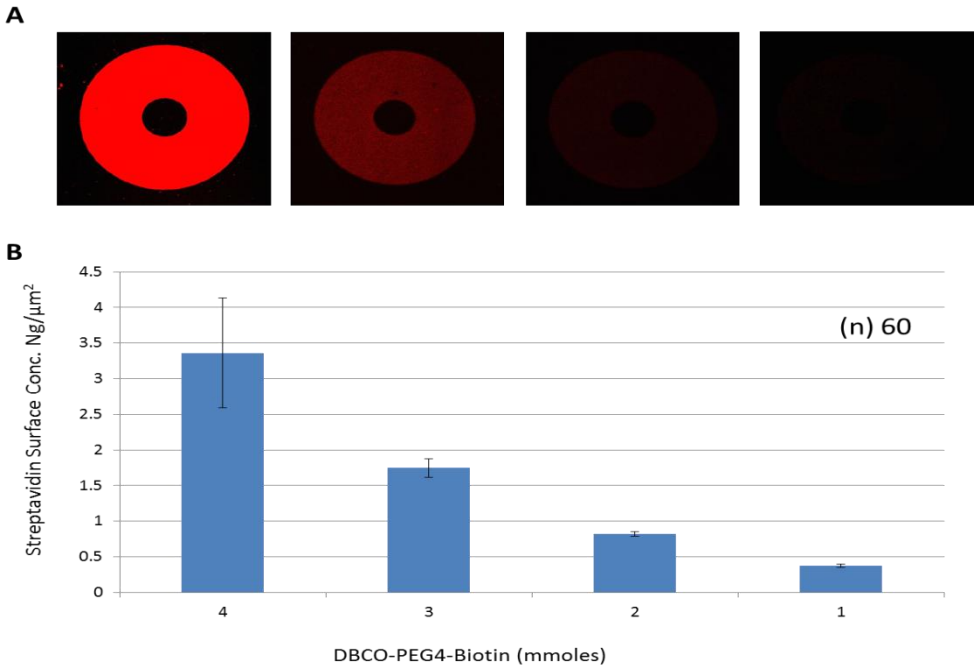

Figure 7: A) Confocal images of streptavidin-546 fluorescent conjugated surfaces at different DBCO-PEG4-Biotin mmoles. B) Quantification of streptavidin-546 fluorescent surface density at different DBCO-PEG4-Biotin mmoles.

3.5 Fidelity and Biocompatibility Evaluation of Robotic Micropatterned Substrates

R-μCP substrates were seeded by hPSCs to analyze biocompatibility and fidelity of hPSCs on cultured on substrates. hPSCs were cultured for 3 days, and brightfield images were taken to assess viability of the cells and quantify micropatten defects (Figure 8). Overall, no cytotoxicity was observed upon seeding and culturing hPSCs on R-μCP substrates. 85% ± 5% of tissues were formed uniformly and consistently inside confined 250 μm diameter circles with 15% ± 5% of tissues demonstrating minimal defects resulted from R-μCP offsets.

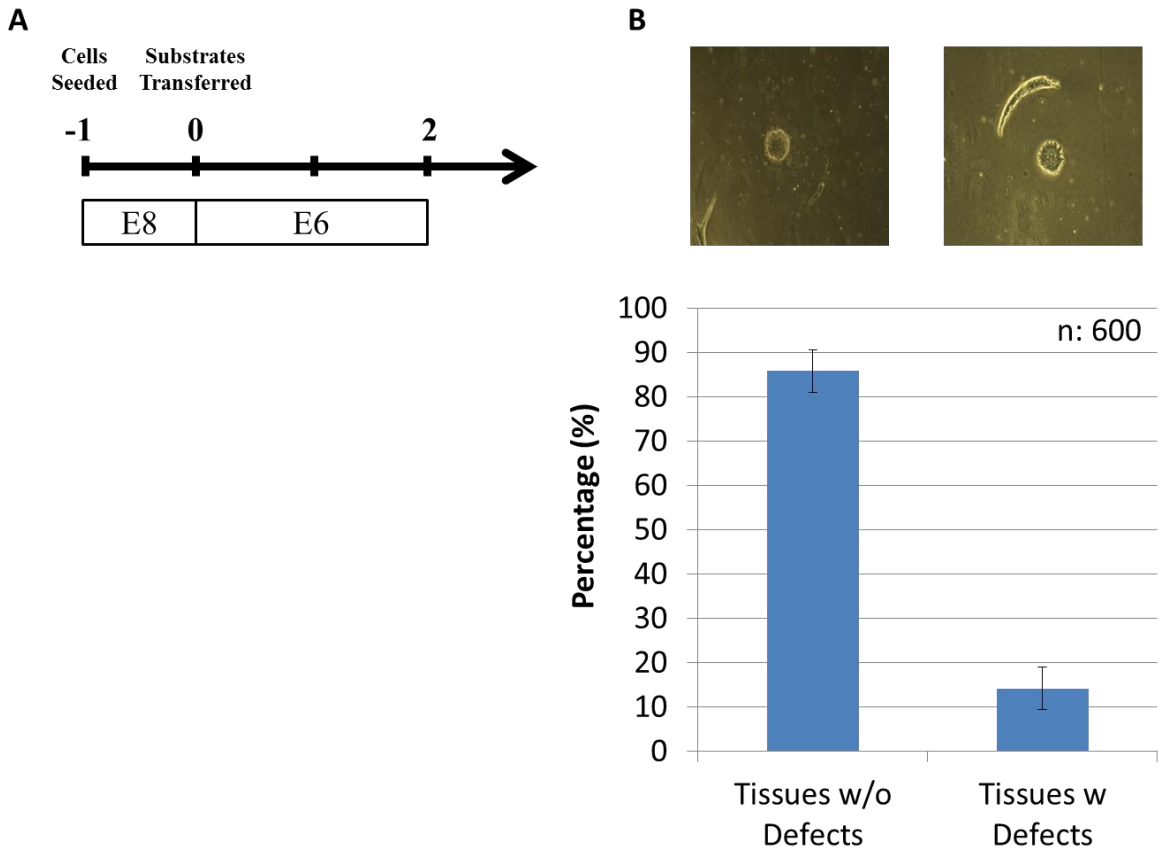

Figure 8: A) Schematic of hPSCs seeding and culturing on R-μCP substrates. B) Quantification of micropattern fidelity on R-μCP substrates with 250 μm diameter adhesive circles and 300 μm radial outgrowth regions.

4 Conclusions

R-μCP system can align patterns of SAMs using PDMS stamps with 15 ± 5 micron accuracy and precision. The intensity and thickness uniformity evaluations of the substrates showed a promising consistency in patterning PEGMA brushes on substrates that can be manually tuned and further modified by small molecules. These R-μCP substrates provide a reliable platform for further advances in tissue expansion. Major advantages of the R-μCP method include the flexibility that it provides in PDMS stamp fabrication and substrate handling as well as scalability due to automation. Substrates can be modified between μCP steps and increase the diversity of functional groups and surface chemistries that can be applied onto custom culture substrates. The primary application of the R-μCP substrates developed in this chapter is to impose spatial and temporal control over single neural rosettes induction and provide a capability to further expand neural rosettes gradually to form complex neural tissues from an original cytoarchitecture.

R-μCP can be further used to engineer biomimetic culture substrates that contain the spatial heterogeneity of microenvironmental cues observed within in vivo tissues. Moreover, robotic micorocantact printing can be used to accurately pattern substrates and facilitate the integration of culture substrates with microfluidics and further enable a scalable manufacturing of novel in vitro assays and microarray screening technologies.

Chapter 3: Optimizing Culture Conditions for Singular Neural Rosette Induction on Tissue Outgrowth Microarrays

1. Introduction

Aggregates of human pluripotent stem cell (hPSC) can be differentiated into neural stem cells (NSCs) and self-organize into biomimetic tissue structures in 2- and 3D culture. In 3D, these neural organoids initiate from structures known as neural rosettes that are comprised of NSCs and recapitulate the apico-basal polarity of the neural tube. The neural tube exhibits simultaneous proliferation of neuroepithelial cells with neuronal differentiation and subsequent radial migration of neuronal progeny to generate tissues with gene expression programs, cell phenotype diversity, and microscale cytoarchitectures mimetic of developing brain and spinal tissues. Therefore, neural organoids have been used to model aspects of human CNS development, physiology, evolution, and neuropathology in manners previously infeasible for model organisms [30, 31, and 38].

However, the spontaneous self-assembly that drives neural organoid morphogenesis also limits the platform's utility to serve as a scalable and reproducible basis for bioengineering tissues that replicate CNS anatomy. Careful attention to details in organoid derivation protocols can ensure reproducibility of their cellular composition. Still, the spontaneous formation of numerous neural rosettes of variable shape and size and at indeterminate locations within the initial NSC aggregates yields an unpredictable and non-mimetic organoid cytoarchitecture at the macroscale. This potentially hinders organoid maturation and renders reproducibility of the organoid's anatomy infeasible [11].

The Ashton lab has already developed substrates capable of singular neural rosette induction. We have already demonstrated that control over the initial microscale morphology of organotypic tissues in 2D culture is critical for this induction. Moreover, we showed that micropatterned substrates in which the size of patterned tissues are systematically controlled can generate singular neural rosette at a higher rate and can be obtained with >80% reproducibility [31, 38] (Figure 1).

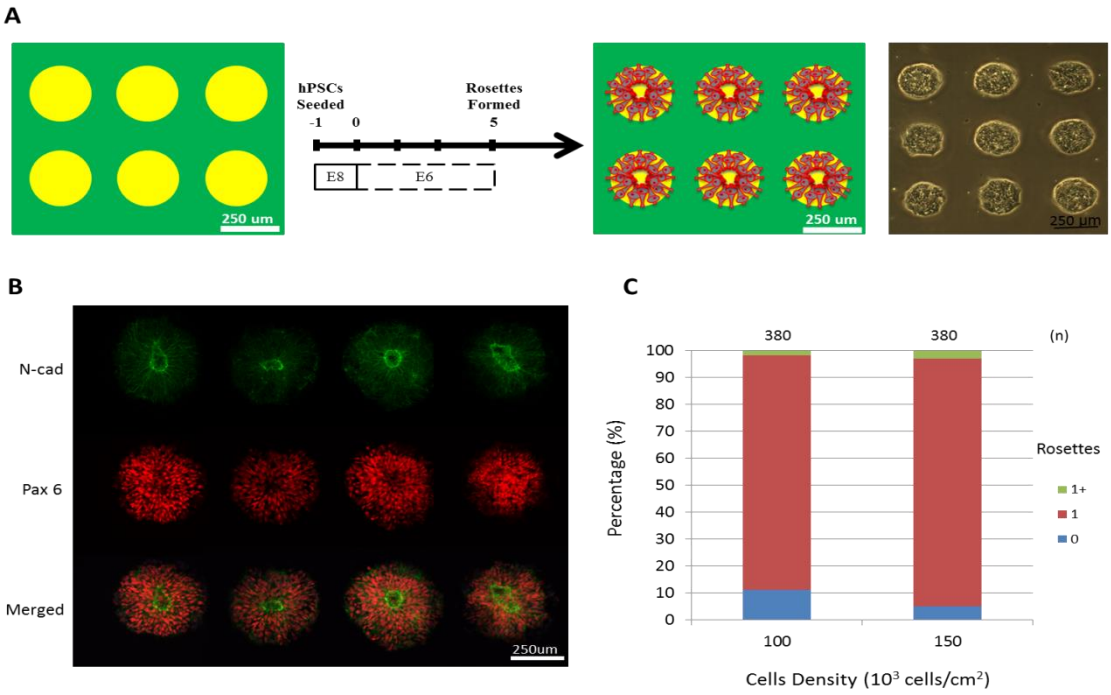

Figure 1: A) Schematic of single rosettes induction from hESCs B) Representative immunostained images of single rosettes on R-μCP outgrowth substrates. 250μm circular adhesive areas (C) Manual quantification of polarization foci/neural rosettes per tissue in three biological replicates with the number of tissues (technical replicates) analyzed per condition indicated above each bar.

In this chapter, we describe a methodology to bioengineer hPSC-derived NSC tissues with controlled induction of a biomimetic singular rosette cytoarchitecture. Control of the NSC aggregates morphology is provided using R-μCP outgrowth culture substrates. Considering the importance of biochemical factors like paracrine signaling molecules and biophysical factors including hPSCs seeding density, we tested whether (1) addition of soluble growth factors and small molecules to direct NSC differentiation and (2) seeding hPSCs at different densities can impact singular neural rosette induction efficiency (Figure 2). These studies allowed us to define a culture protocol for effective singular neural rosettes induction on R-μCP, tissue outgrowth culture substrates. The resulting rosette tissues on R-μCP culture substrates model the cytoarchitecture of a transverse slice of the embryonic neural tube.

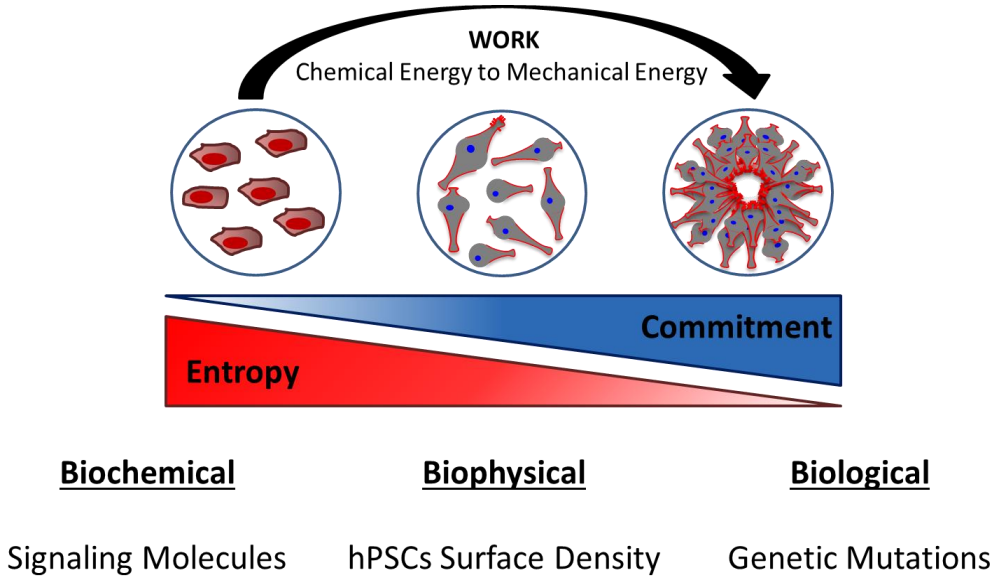

Figure 2: Schematic of single rosettes induction from hESCs and various parameters involved in this process.

Reproducible derivation of NSC tissues with a singular rosettes cytoarchitecture represents a promising first step in bioengineering neural organoids with biomimetic CNS anatomy. Integration of these methods with patterning and surface chemistry techniques coupled with microfluidic devices and genetically engineered hPSCs can enable additional spatiotemporal control of neural organoid morphogenesis and can further advance the field toward the next-generation neural organoids that reproducibly replicate CNS anatomy, circuitry, and thereby physiology.

2. Materials and Methods

2.1 Materials

H9 human embryonic stem cells (hESCs) along with bFGF were provided from WiCell. Gibco™ Essential 8™ Medium, Gibco™ Essential 6™ Medium, DMEM/F-12 Medium, Tissue-culture polystyrene (TCPS) plates, Versene, Phosphate buffered saline (PBS) and secondary Alexa Fluor™ antibodies were purchased from ThermoFisher. ROCK inhibitor Y-27632 and TGFβ were provided from R&D Systems. Growth factor-reduced Matrigel at variable concentrations were bought from BD Biosciences. SB-431542 and LDN-193189 were provided from cayman. Dimethyl sulfoxide, 4% Paraformaldehyde (in PBS), Tris-Buffered Saline (TBS), Donkey serum, Triton X-100 were provided from Sigma-Aldrich. Primary antibodies Rabbit Anti-Pax6, Mouse Anti-N-cadherin and 6-Diamidino-2-phenylindole (DAPI) were provided from Invitrogen. Anti-Fade Reagent was purchased from Molecular Probes. All other materials and reagents not labeled with a source denotation were purchased from Fisher and used as received.

2.2 Matrigel Coating of R-μCP substrates

R-μCP outgrowth substrates developed in chapter 2 were rinsed five times with sterile PBS in a biosafety cabinet. Substrates were transferred to an individual well of a new 6-well TCPS plate using tweezers. 12 mL of DMEM/F12 media was added to a 15-mL conical. 1 mL of media from the conical was added to each well of a 6-well plate. Matrigel aliquots were thawed at room temperature until the pellet is slightly melted. 1 mL of DMEM/F12 was removed from the 15 mL conical and used to further dissolve the Matrigel pellet. The matrigel suspension was further diluted in the remaining DMEM/F12 media in the 15 mL conical by pipetting up and down several times. 1 mL of the dissolved Matrigel solution was added to each well of the plate, and Matrigel coating of the substrates proceeded overnight in a 37 ˚C cell culture incubator.

2.3 hPSCs culturing

One vial of hPSCs was removed from liquid nitrogen storage. The vial was placed at room temperature for 60 seconds, and then manually warmed in hand for another 15 seconds. Next, the vial was swirled in the water bath until it was approximately 75% thawed and transferred to a sterilized biosafety cabinet. The content of the vial was gently transferred to a 15-mL conical using a 2-mL glass pipette and 4 mL of E8 medium was added to it dropwise. The cell suspension was spin down for 5 min at 1000 rpm. The supernatant was aspirated, and the pellet was resuspended in 12 mL of E8 medium containing 10 μM Y27632, a.k.a. Rock inhibitor. Two milliliters of cell suspension was added into each well of a 6-well TCPS plate and was placed in incubator shaking side to side and then back and forth to distribute the cells evenly. 100% of E8 medium was changed daily thereafter. Cells should be ready to passage after approximately 4–5 days of culture depending on the density at which they are seeded. Cells are ready to passage

when the plate is ~80% confluent or when colonies have become so large that debris begins to accumulate in the middle of the colonies.

2.4 Generation of Micropatterned Forebrain Neural Rosette Arrays

hPSCs were rinsed at 80% confluency with PBS and were dissociated with 1 ml Accutase for 5 min at 37 ˚C. Singularized cells in Accutase were the collected using a pipette and were transfer into a conical tube with 6 mL of E8 media. The conical tube was centrifuged at 1000 rpm for 5 min. The hPSCs were resuspended in E8 media with 10 mM ROCK inhibitor. hPSCs were seeded onto micropatterned coverslips at 100,000 cells/cm^2 using 4 mL of media per well on day -1. 4 mL E6 was added to each well of a new 6-well TCPS plate on Day 0. R-μCP hPSC-seeded substrates were transferred into a new well containing E6 media and were maintained. On Day 1, 2 mL of E6 media was aspirated from each well and 2 mL of fresh E6 media was added to each well (50% media change). 50% media changes were performed daily until Day 5.

2.5 Immunostaining to Detect Singular Neural Rosettes Induction

Tissue arrays were washed with PBS to remove cell debris prior to fixation. 50% PBS washes was used to avoid lifting tissues from the array surface. Cells were fixed in 4% paraformaldehyde for 10 min at room temperature. Cells were washed 2–3 times in PBS to remove excess PFA. 50% media changes were performed to avoid lifting cells from surface of plate/slide for all wash steps. Cells were blocked and permeabilized in TBS-DT for at least 1 hour at RT. Then, tissues were incubated with rabbit anti-Pax6 and mouse anti-N-cadherin primary antibodies diluted in fresh TBS-DT. This step may be performed overnight at 4 ˚C. Tissues are the washed 2–3 times in TBST for 10 min each on a rocker. Tissues were incubated

with appropriate Alexa Fluor secondary antibodies at a 1:500 dilution in the dark for at least 2 hour at RT. Tissues were washed two times with TBS for 15 min each on rocker. Diluted DAPI solution (1:2000 DAPI stock solution into TBS; stored in foil at 4 ˚C) was added to each well and was incubated for 10 min at RT to stain nuclei with DAPI. Tissues were then washed with TBS for 15 min and fresh TBS to was added to well-plates and stored at 4 ˚C until mounting. 50-μL droplet of anti-fade reagent (PVA-DAPCO) was placed on a microscope coverslide and the R-μCP substrate was mounted on the coverslip. It was left in the dark at room temperature overnight to dry. Edges of R-μCP substrate were sealed to the microscope coverslide with clear nail polish before imaging. Bright field and confocal microscopy images were acquired at 40x magnification. Tissues were further analyzed to quantify number of tissues with singular rosette induction.

2.6 Analysis of Culture Media and hPSCs Seeding Density for Singular Neural Rosettes

hPSCs were seeded onto micropatterned coverslips at 100K and 50K cells/cm^2 using 4 mL of media per well on day -1. E6 media (4 mL)was added to each well of a new 6-well TCPS plate on Day 0. R-μCP hPSC-seeded substrates were transferred into a new well containing E6 media and were maintained. Solutions of fresh E6 media, fresh E6 media containing FGF2 20 ng/mL, fresh E6 media containing dual SMAD inhibitors, 100nM LDN and 10uM SB, were prepared as culture media conditions. A conditioned media consisting of 50% fresh media and 50% media from neural progenitors seeded at 150K cells/cm^2 in a standard 6 well plate was also prepared. On Day 1, 2 mL of E6 media was aspirated from each well. 2 mL of each culture media condition was added to each well (50% media change). 50% media changes were performed daily until Day 5.

3. Results and Discussion

3.1 Conditioned Media Impacts Neural Rosette Induction

Single neural rosettes induction on R-μCP substrates was performed by seeding hPSCs and culturing in standard E6 protocol. Upon completion of E6 protocol, immunostaining and quantification of neural tissues was performed to quantify singular neural rosette induction on R-μCP substrates and an efficiency of 20% ±3% was obtained (Figure 3). This obtained singular neural rosette induction efficiency is lower than the efficiency that was previously recorded on standard micropatterned substrates in Figure 1.

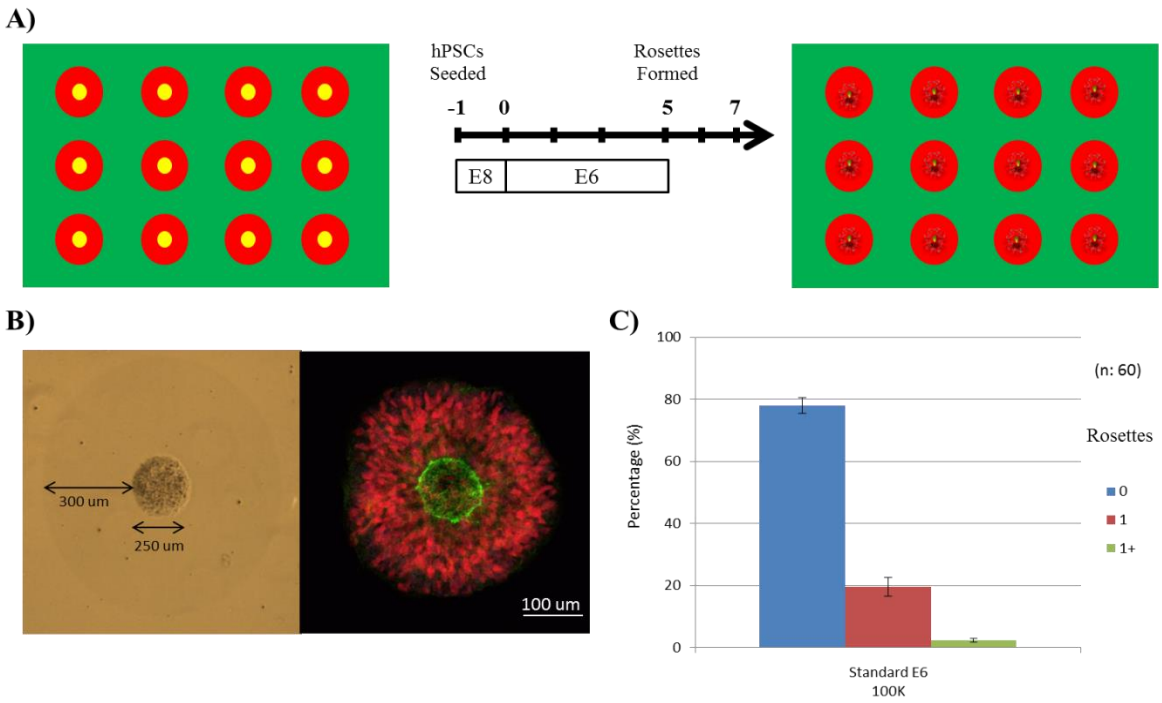

Figure 3: A) Schematic of single rosettes formation from hESCs seeded at 100k cells/cm^2 on R-μCP substrates B) Representative immunostained images of single rosettes on R-μCP outgrowth substrates. 250 μm adhesive circles and 300 μm outgrowth regions. (C) Manual quantification of polarization foci/neural rosettes per tissue in three biological replicates with the number of tissues (technical replicates) analyzed per condition indicated above each bar.

We hypothesized addition of soluble growth factors and small molecules to direct NSC differentiation may also vary efficiency of singular neural rosette induction. FGF2, also known as basic fibroblast growth factor, is a growth factor and signaling protein encoded by the FGF2 gene. FGF2 is secreted from cells through an unconventional secretory mechanism and is necessary for cell proliferation and neurogenesis in the developing cerebral cortex [34, 35]. Dual SMAD inhibitors, Noggin and SB431542, are also known to derive neural progenitor cells from hPSCs and yield to rapid differentiation of hPSCs into highly conditioned population of NSCs [36, 37]. Considering the importance of cell density-dependent paracrine signaling molecules, we also included a conditioned media condition consisting of 50% fresh media and 50% media from neural progenitors seeded at 150K in a standard 6 well plate (Figure 4).

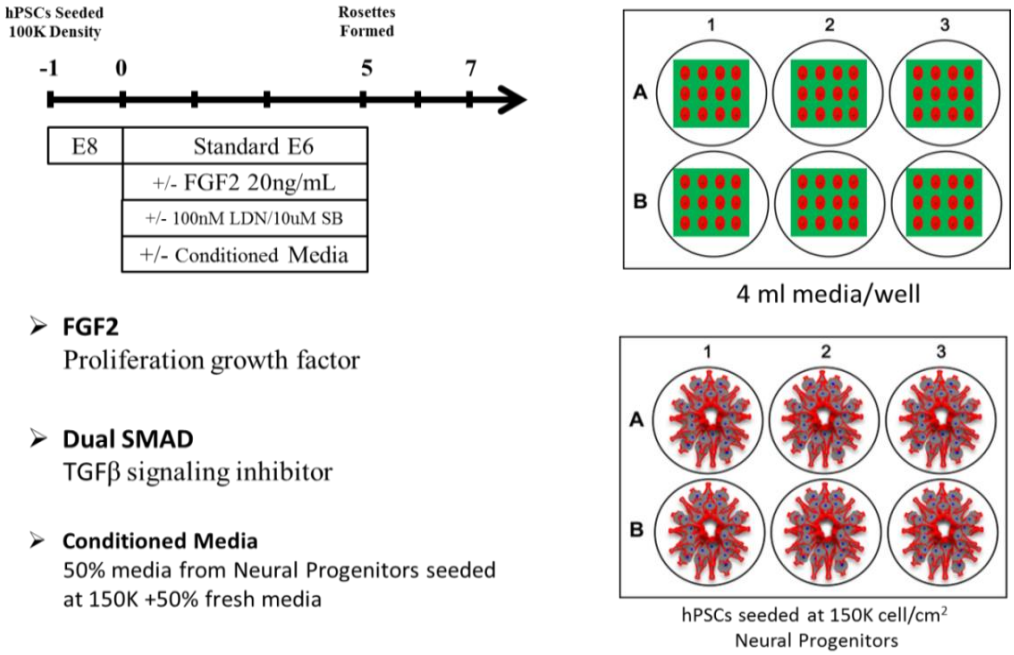

Figure 4: Schematic of single rosettes induction from hESCs on R-μCP substrates under different culture conditions. 250 μm diameter adhesive circles and 300 μm outgrowth regions.

After generating neural tissue arrays under each media condition, the arrays were stained and imaged using confocal microscopy. Addition of dual SMAD 100nM LDN and 10uM SB or FGF2 20ng/mL inhibitors to E6 culture media did not yield to higher neural rosettes induction and generated 1% ±1% and 5% ±2% singular neural rosettes respectively. Most of the tissues formed under these culture conditions were characterized with abnormal morphologies. Quantification of neural tissues formed under conditioned media, containing 50% media from neural progenitors seeded at 150K in a standard 6 well plate, yielded significantly higher percentage of singular neural rosettes at 40% ±5% efficiency compared to standard E6 condition at 15% ±5%. It can be concluded that conditioned media can compensate for the low concentration of signaling molecules secreted by the cells seeded on R-μCP outgrowth substrates and can improve singular neural rosette induction efficiency (Figure 5).

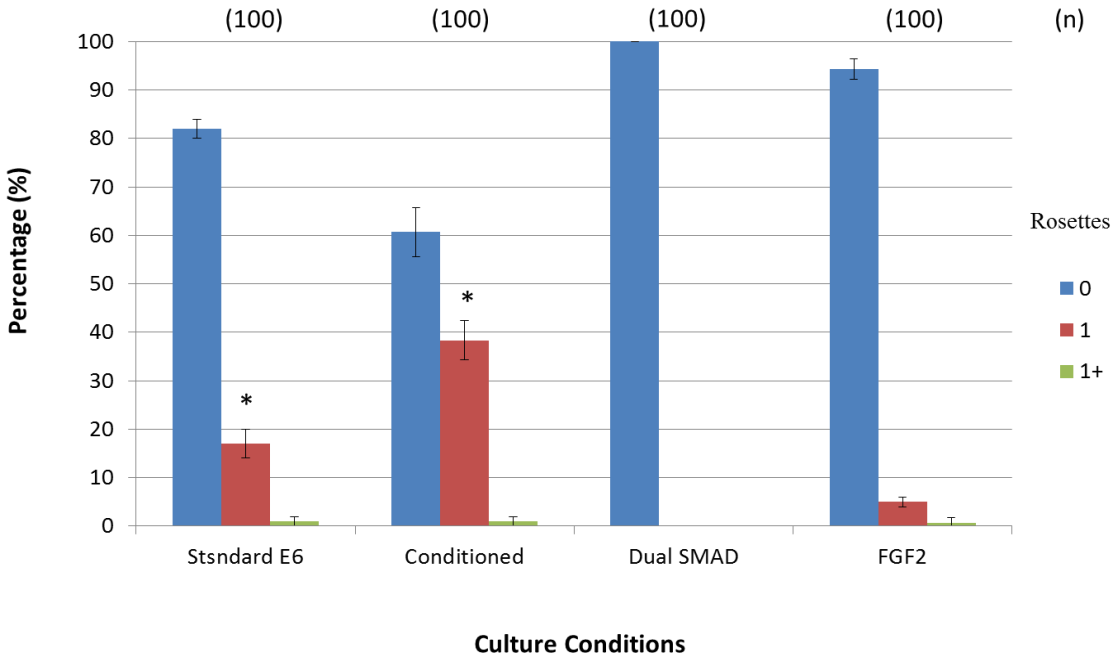

Figure 5: Manual quantification of polarization foci/neural rosettes per tissue with the number of tissues (technical replicates) analyzed per condition indicated above each bar. (*) indicates a significance of $p<0.05$ calculated using a One-way ANOVA.

3.2 Cells Seeding Density Impacts Neural Rosette Emergence

Since hPSCs are mainly responsible to proliferate and differentiate to form neural rosettes on R-μCP outgrowth substrates, we hypothesized initial hPSCs seeding density can impact singular neural rosette induction. In order to test our hypothesis, we seeded hPSCs at densities of 100,000 and 50,000 cells/cm^2 on R-μCP substrates under conditioned media culture. Tissues formed at 50,000 cells/cm^2 hPSCs seeding density started with smaller cellular aggregates on day 0 and generated 60% ±5% singular neural rosettes on day 5. Tissues formed at 100k hPSCs seeding density under the same conditioned culture media started with relatively bigger cellular aggregates on day 0 and generated 40% singular neural rosettes on day 5 (Figure 6).

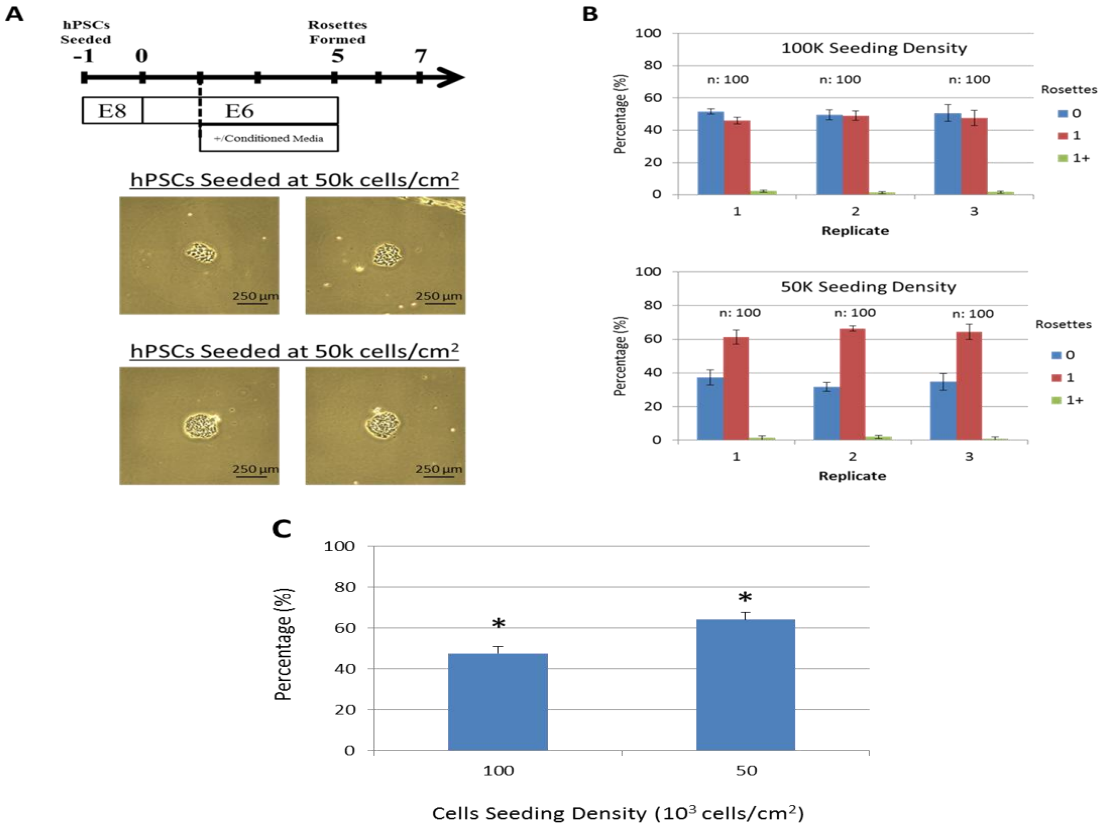

Figure 6: A) Schematic and brightfield images of hESCs seeded at different densities. B) Manual quantification of polarization foci/neural rosettes per tissue with the number of tissues (technical replicates) analyzed per condition indicated above each bar. C) Average singular rosette emergence over the three trials at different densities. (*) indicates a significance of $p<0.05$ calculated using a One-way ANOVA.

4. Conclusions

The R-μCP outgrowth substrates developed in chapter 1 were able to direct formation of neural rosettes of uniform shape and morphology but were limited to only 20% ±3% singular neural rosette induction efficiency. Singular neural rosette induction efficiency is dependent on multiple variables. As we suspected, singular neural rosette induction efficiency is related closely with the culture media composition. Initial hPSCs seeding density is also another important factor in singular neural rosette induction efficiency. We evaluated the self-organization capacity of NSCs into singular neural rosettes on R-μCP outgrowth substrates under different culture media conditions and at different hPSCs seeding densities. Results of repeated experiments using conditioned culture media yielded 40% ±5% singular neural rosettes induction. This efficiency is significantly higher than 20% ±3% efficiency in singular neural rosette induction that was obtained initially using standard E6 protocol.

hPSCs seeding density is another parameter that can improve singular neural rosette induction efficiency [31]. Results of repeated experiments using conditioned culture media and 50k cells/cm^2 hPSCs seeding density yielded in 64% ±3% singular neural rosettes induction. This efficiency is significantly higher than 47% ±3% efficiency that was obtained using conditioned culture media and 100k cells/cm^2 hPSCs seeding density. Therefore, R-μCP outgrowth substrates developed in chapter 2 can generate arrays of correctly polarized singular neural rosettes with 60% efficiency using conditioned culture media and 50k cells/cm^2 hPSCs seeding density (Figure 7).

Although conditioned media composition is not well characterized and its composition is unknown, the improvement in efficiency using conditioned media makes it worth to note that an optimal combination of known signaling molecules and growth factors at different concentrations might help with higher singular neural rosette induction. The characterization of conditioned media and analysis of its composition can potentially be used to further optimize the culturing media and develop a defined enriched media that can be used in combination with different hPSCs seeding density to yield higher singular neural rosette induction efficiency.

Another parameter that is suspected to be essential in singular neural rosette induction on R-μCP outgrowth substrates is the ECM protein that hPSCs are seeded on. Here, Matrigel protein was used for coating R-μCP outgrowth substrates prior to seeding hPSCs. Matrigel is an ill-defined matrix and although it has been used widely in hPSCs culturing it is not a reliable protein mixture and can also be a source of variability [39]. We assume replacing Matrigel with a well-defined protein or adhesive peptide sequence like RGD can potentially improve singular neural rosette induction efficiency on R-μCP outgrowth substrates.

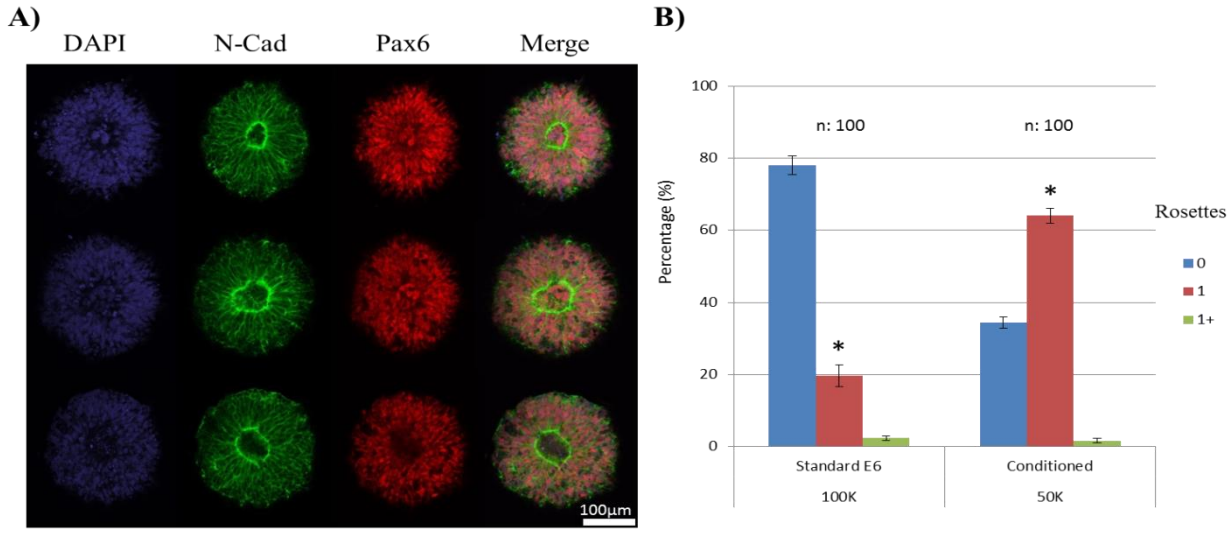

Figure 7: A) Representative immunostained images of single rosettes on R-μCP substrates. B) Manual quantification of polarization foci/neural rosettes per tissue in three biological replicates. (*) indicates a significance of $p<0.05$ calculated using a One-way ANOVA.

Chapter 4: Spatially and Temporally Controlled Expansion of Single Neural Rosettes to Create Bioengineered Tissue Slices

1. Introduction

CNS development begins with formation of the primordial neural tube spanning the rostro-caudal (R/C) axis of the dorsal embryo surface. The neural tube serves as the primordial anlage for all neuronal and glial cells of the developing CNS. It is morphologically characterized by a single layer of columnar neuroepithelial cells exhibiting trademark apical polarization of N-cadherin and basal deposition of a laminin-rich basal lamina (Chapter 1, Figure 3) [12].

The neural tube expands radially via simultaneous differentiation and migration of neuroepithelial cell progeny. Neuroeptihelial cells remain at the apical boundary of the tissue undergoing an asymmetric cell division phenomenon known as interkinetic nuclear migration (IKNM). The actions of the cytoskeleton during neuroepithelial cell mitosis and subsequent radial expansion of the tissue, vary depending on the location along the neural tube's R/C axis. In forebrain regions of the neural tube, neuroepithelial cells differentiate into radial glial cells that maintain cell-cell interactions at the apical surface while extending processes to the readily expanding basal boundary. Radial glial cells are maintained as a pool of neural progenitors throughout embryonic development [13, 14]. A balance of cell-cell and cell-extracellular matrix (ECM) interactions is thought to play a role in facilitating forebrain development into the classic stratified cerebral cortical structure (Figure 4, Chapter 1) [15].

Our lab recently published methods for engineering culture substrates that enable micropatterning of single neural rosette tissues and temporal control of their radial outgrowth [31]. Outgrowth of 200μm diameter tissues at 400μm center-to-center spacing generated tissues

with a singular neural rosette cytoarchitecture that maintained apico-basal polarity. These micropatterned substrates yielded tissues with an apically polarized population of NECs but due to lack of controlled tissue outgrowth they exhibited loss of apico-basal polarity and uncontrolled neuronal migration (Figure 1).

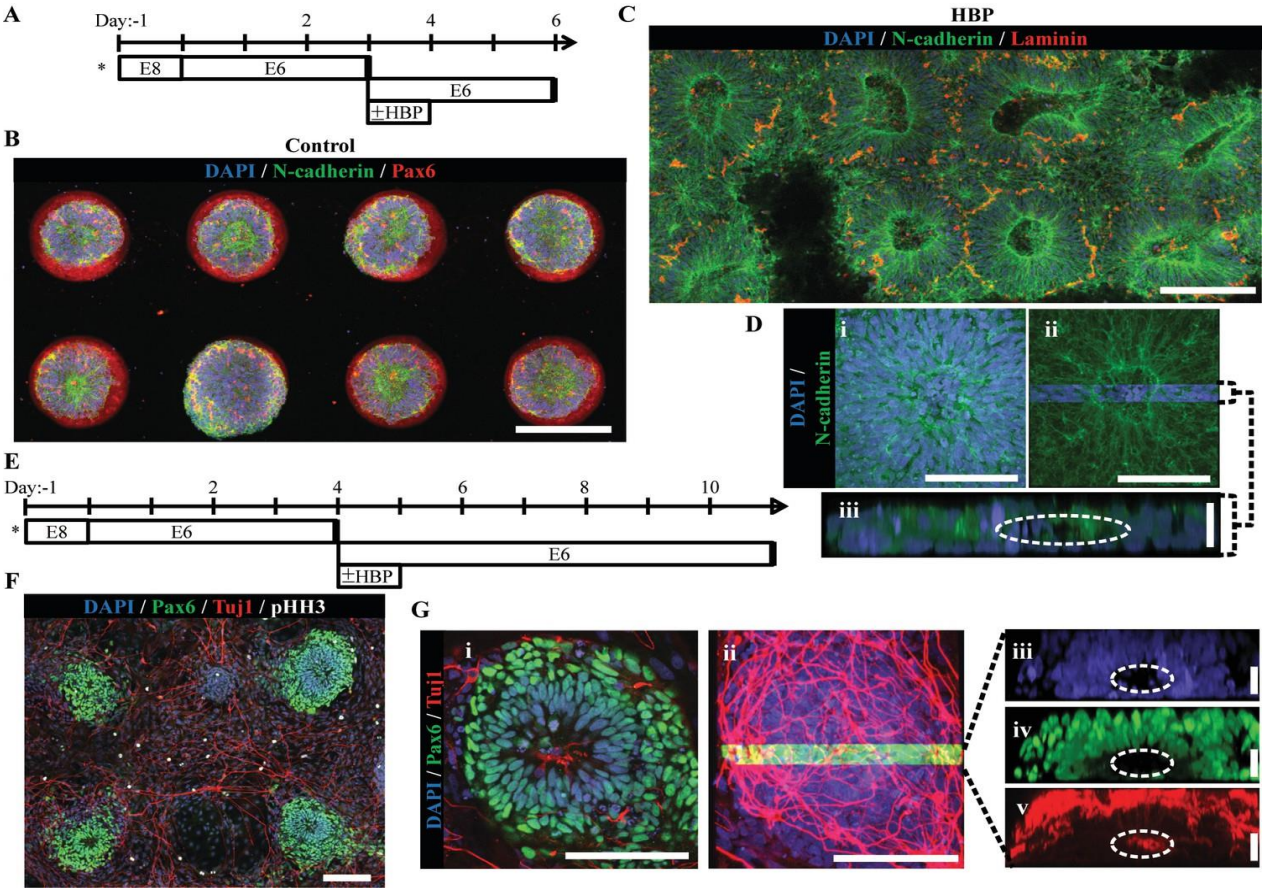

Figure 1: A) Schematic for derivation and HBP-mediated expansion of forebrain neuroepithelial tissues on micropatterned arrays of 200μm diameter circles with 400μm center-to-center spacing. B) Image of singular neural rosette emergence within D6 neuroepithelial tissues on micropatterned substrates. C) Image of singular neural rosette expansion within D6 neuroepithelial tissues on micropatterned substrates functionalized with HBP-DBCO bioconjugates. D) (i) Magnified image of expanded neuroepithelial tissue with (ii) highlighted 3D cross-section and (iii) profile view; white dotted line indicates hollow polarization cavity.

Figure 1 continue: E) Schematic for derivation and HBP-mediated expansion of forebrain neural tissues on micropatterned arrays of 200 μm diameter circles with 800 μm center-to-center spacing. F) Image of singular neural rosette tissue outgrowth and neuronal differentiation on HBP-functionalized substrates at day 11. (G) (i) Magnified image of the neuroepithelial center of expanded neural tissues with (ii) the highlighted 3D cross-section and profile view of (iii) nuclei, (iv) Pax6+ core, and (v) primarily peripheral Tuj1+ neuronal processes; white dotted lines indicate hollow polarization cavity [31].

In this chapter, we use R-μCP substrates to exert spatiotemporal control over the radial expansion of micropatterned neural rosette tissues. R-μCP substrates capable of directing fixed areas of cell outgrowth will be designed as arrays of chemically modifiable annuli with 250μm internal diameter (ID) and 300μm outer diameters (OD). The surrounding substrate surface area will be rendered inert thus limiting functionalization of the culture surface to the printed annuli, which will be further functionalized with azide groups and can present arrays of correctly polarized singular neural rosettes. CGYGPGRGDSPK (RGD) peptide, an integrin-binding peptide sequence, can mediate cell adhesion through a wide variety of integrin ligands but potentially interfere with cell-ECM interactions at the basal surface of micropatterned neural tissues [30]. As such, we expect substrate functionalization with a heparin-binding peptide CGTYRSRKY (HBP), known to promote native ECM deposition, can facilitate cell-mediated environment remodeling and can more accurately recapitulate neural tissue expansion [31].

Upon generation of singular neural rosettes on R-μCP substrates and conjugation with bioactive cell adhesion-promoting peptides in situ, NSCs migration was studied and an optimal bioconjugation condition was developed to maintain dynamic polarized rosette morphology while enabling radial migration of neural progeny. Functionalization of R-μCP substrates with

cell adhesion molecules will allow for cell-mediated and spatially defined radial migration of naturally differentiated neuronal tissues.

2. Materials and Methods

2.1 Materials

Resin-YKRSRYTGG-Fmoc, CGTYRSRKY and CGYGPGRGDSPK peptide sequences were purchased from Genescript. DBCO-PEG4-Maleimide and DBCO-PEG4-Acid where provided form Click Chemistry Tools. Bio-Gel P-2 Gel was purchased from Bio-Rad. H9 human embryonic stem cells (hESCs) with bFGF were provided from WiCell. Gibco™ Essential 8™ Medium, Gibco™ Essential 6™ Medium, DMEM/F-12 Medium, Tissue-culture polystyrene (TCPS) plates, Versene, Phosphate buffered saline (PBS) and secondary Alexa Fluor™ antibodies were purchased from ThermoFisher. ROCK inhibitor Y-27632 and TGFβ were provided from R&D Systems. Growth factor-reduced Matrigel at variable concentrations was bought from BD Biosciences. Dimethyl sulfoxide, 4% Paraformaldehyde (in PBS), Tris-Buffered Saline (TBS), Donkey serum Triton X-100, Tris(2-carboxethyl)phosphine hydrochloride (TCEP), 2-(6-Chloro-1-H-benzotriazole-1-yl)-1,1,3,3-tetramethylaminium hexafluorophosphate (HCTU), DMF, DMSO were provided from Sigma Aldrich. Accutase, Primary antibodies: Rabbit Anti-Pax6, Mouse Anti-N-cadherin and 6-Diamidino-2-phenylindole (DAPI) were provided from Invitrogen. Anti-Fade Reagent was purchased from Molecular Probes. All other materials and reagents not labeled with a source denotation were purchased from Fisher Scientific and used as received.

2.2 Synthesis of DBCO Peptide Conjugates via Michael-type Addition Chemistry

Peptides were added to a solution of Tris (2-carboxethyl) phosphine hydrochloride (TCEP) in sterile water at pH 7.0 for 1 hr at room temperature. DBCO-PEG4-Maleimide in DMF was

added to the solution in 4:1 molar excess andreacted while shaking for 2 hr at room temperature. The reaction was the pipetted onto the gel bed of a size-exclusion chromatography (SEC) column packed with Bio-Gel P-2 Gel (Bio-Rad) and allowed to enter the column under gravity flow. The reaction solution was passed through the column using 100 mL sterile water and eluted into a hundred 1 mL aliquots. Aliquots were then concentrated via freeze-drying and analyzed with UV-Vis spectrophotometry at 309nm wavelength, which corresponded to the presence of DBCO. A Micro-BCA Assay (Promega) was also performed on aliquots to track the presence of peptide conjugates. UV-Vis measurements of known DBCO concentrations were used to generate a standard curve and for quantification of peptide-PEG4-DBCO conjugate concentrations. Peptide conjugate aliquots were stored lyophilized at 20˚C and resuspended in PBS before use.

2.3 Synthesis of DBCO Peptide Conjugates on Resin

Resin-YKRSRYTGG-Fmoc was purchased from Genescript and was transferred to a hand coupling vessel. 5 mL of 20% piperidine was added to the vessel to deprotect Fmoc group from the amino acid on the resin. Solution was mixed for 5 mins by bubbling in nitrogen gas. An excess amount of DBCO-PEG4-COOH and coupling agent (HCTU) were dissolved in 20% N-methylmorpholine in DMF or 20% collidine in DMF. Solutions of DBCO-PEG4-COOH /coupling agent was added onto the resin in vessel and was mixed on a shaker overnight. After coupling was completed the final peptide conjugate was cleaved with 20% piperidine in DMF and was washed 3 times with DMF. Analytical HPLC was used to analyze DBCO conjugated peptide (Figure 2).

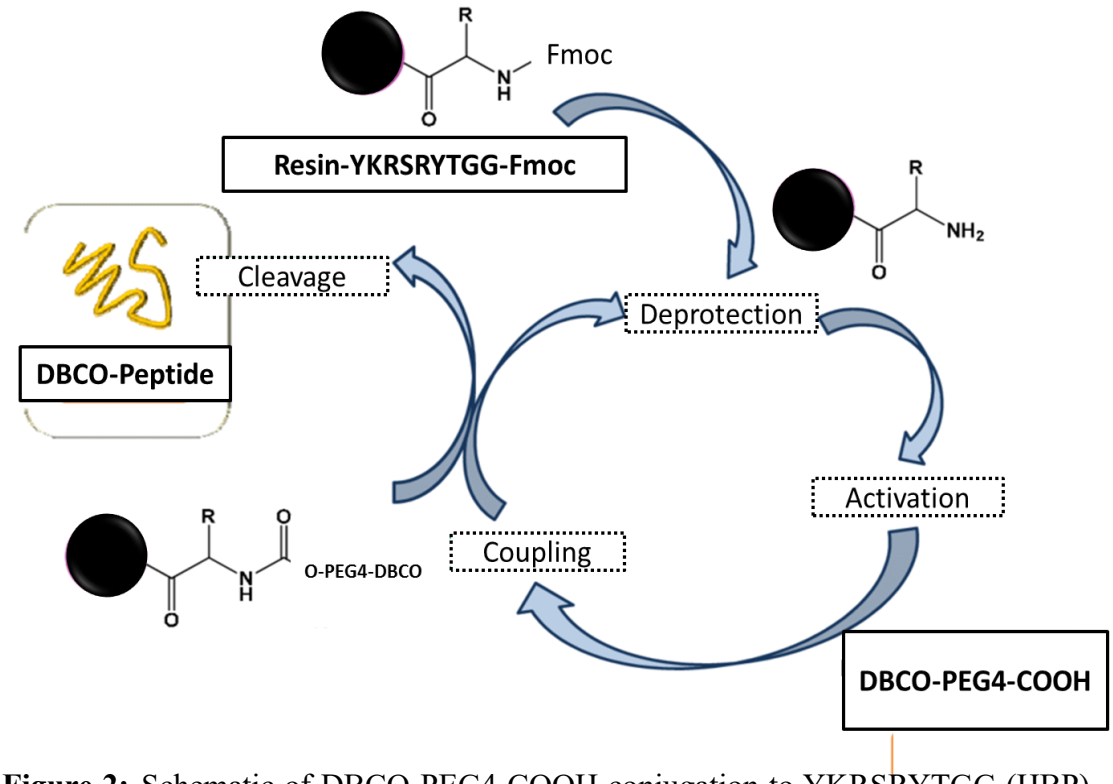

Figure 2: Schematic of DBCO-PEG4-COOH conjugation to YKRSRYTGG (HBP) on a resin. (R) Indicates side alkyl groups.

2.4 DBCO Peptide Surface Conjugation and XPS Characterization

In situ modification of R-μCP substrates was performed by incubating an azide-functionalized micropatterned coverslip in 2 ml of DBPS containing 15 μM DBCO-PEG4-Peptide. The reaction was allowed to proceed for 24 hr at room temperature. Substrates were rinsed 5 times with DPBS upon completion. XPS measurements were performed using a Thermo Scientific Model K-Alpha XPS instrument with monochromatic Al Kα radiation (1486.7 eV). Survey spectra and high-resolution spectra for N1s were acquired using analyzer pass energies of 200 and 50 eV, respectively, with an X-ray spot size of 50μm for single point analysis. Data was analyzed using Avantage XPS software package and peak fitting with Gaussian/ Lorentzian peak shapes and a Shirley/Smart type baseline.

2.5 In Situ Expansion of Neural Rosette Tissues

After seeding hPSCs on R-μCP substrates, arrays of single neural rosettes were generated as previously described in Chapter 3. On Day 3 of neuroepithelial tissue generation, E6 media was supplemented with DBCO-peptide conjugates at 1 μM, 5 μM, 10 μM, 15 μM. After 24 hrs, a routine 50% media change was performed and daily media changes afterwards until Day 7. R-μCP NSC tissue arrays were washed with PBS to remove cell debris prior to fixation. 50% PBS washes was used to avoid lifting tissues from surface. Cells were fixed in 4% paraformaldehyde for 10 min at room temperature. Cells were washed 2–3 times in PBS to remove excess PFA. 50% media changes were performed to avoid lifting cells from surface of plate/slide for all wash steps.

2.6 Immunostaining of Neural Tissues

Cells were blocked and permeabilized in TBS-DT for at least 1 hour at RT. Arrayed tissues were then incubated with rabbit anti-Pax6 and mouse anti-N-cadherin primary antibodies diluted in fresh TBS-DT overnight at 4 ˚C. Arrays were washed 2–3 times in TBST for 10 min each on a rocker, and then incubated with appropriate Alexa fluor secondary antibodies at a 1:500 dilution in the dark for at least 2 hour at RT. Next, arrayed tissues were washed two times with TBS for 15 min each on rocker. Diluted DAPI solution (1:2000 DAPI stock solution into TBS) was added to each staining solution, and the arrays were incubated for 10 min at RT to stain cell nuclei. Afterwards, the arrays were washed with TBS for 15 min and fresh TBS to was added to well-plates and stored at 4 ˚C until mounting. For mounting, 50-μL droplet of anti-fade reagent (PVA-DAPCO) was placed on a microscope coverslide and the R-μCP substrate was mounted on the coverslip. It was left in the dark at room temperature overnight to dry. Edges of R-μCP substrate

were sealed to microscope coverslide with clear nail polish before imaging. Confocal microscopy was used to capture 40x magnification images. Tissues were further analyzed to quantify the number of tissues displaying singular neural rosette induction.

3. Results and Discussion

3.1 Clickable Peptide Conjugates Purification and Quantification

CGYGPGRGDSPK (RGD) peptide is an integrin-binding peptide sequence, which mediates cell adhesion through a wide variety of integrin ligands and can potentially interfere with cell-ECM interactions at the basal surface of micropatterned neural tissues [30]. CGTYRSRKY (HBP) is a heparin-binding peptide known to promote native ECM deposition and capable of remodeling an culture microenvironment for neural tissue expansion [33]. DBCO–PEG4–Maleimide linkers were conjugated to RGD and HBP peptide sequences containing a cysteine residue via Michael-type addition using a 4:1 molar excess of DBCO–PEG4–Maleimide. The DBCO-RGD conjugates were isolated using size exclusion chromatography and UV-Vis spectroscopy based on 309 peak characteristic of DBCO (Figure 3).

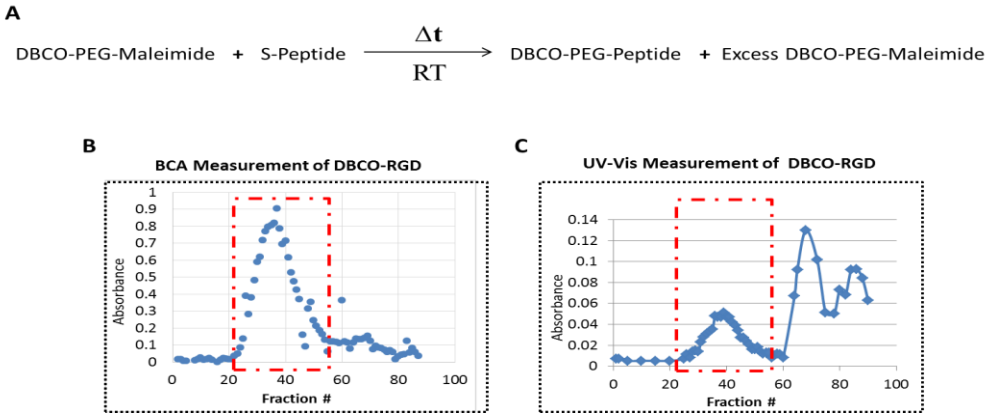

Figure 3: Schematic of DBCO-PEG-Maleimide conjugation to RGD peptide. B) micro BCA assay at 495 nm C) size exclusion chromatography traces of DBCO-RGD cogugates quantified at 309 nm in 1 ml fractions. Red dotted box indicates alignment of RGD peptide and DBCO elution in fractions containing the desired DBCO-RGD conjugates.

After having difficulties in synthesis and purification of DBCO-HBP conjugates via Michael-type addition, a DBCO-PEG4-COOH linker was conjugated to a Resin-YKRSRYTGG-Fmoc after deprotection of Fmoc groups. DBCO-HBP conjugates were then washed excessively on the resin to remove all unreacted reagents and were cleaved. DBCO-HBP conjugates were purified using an analytical HPLC and a synthesis efficiency of 78% was quantified (Figure 4).

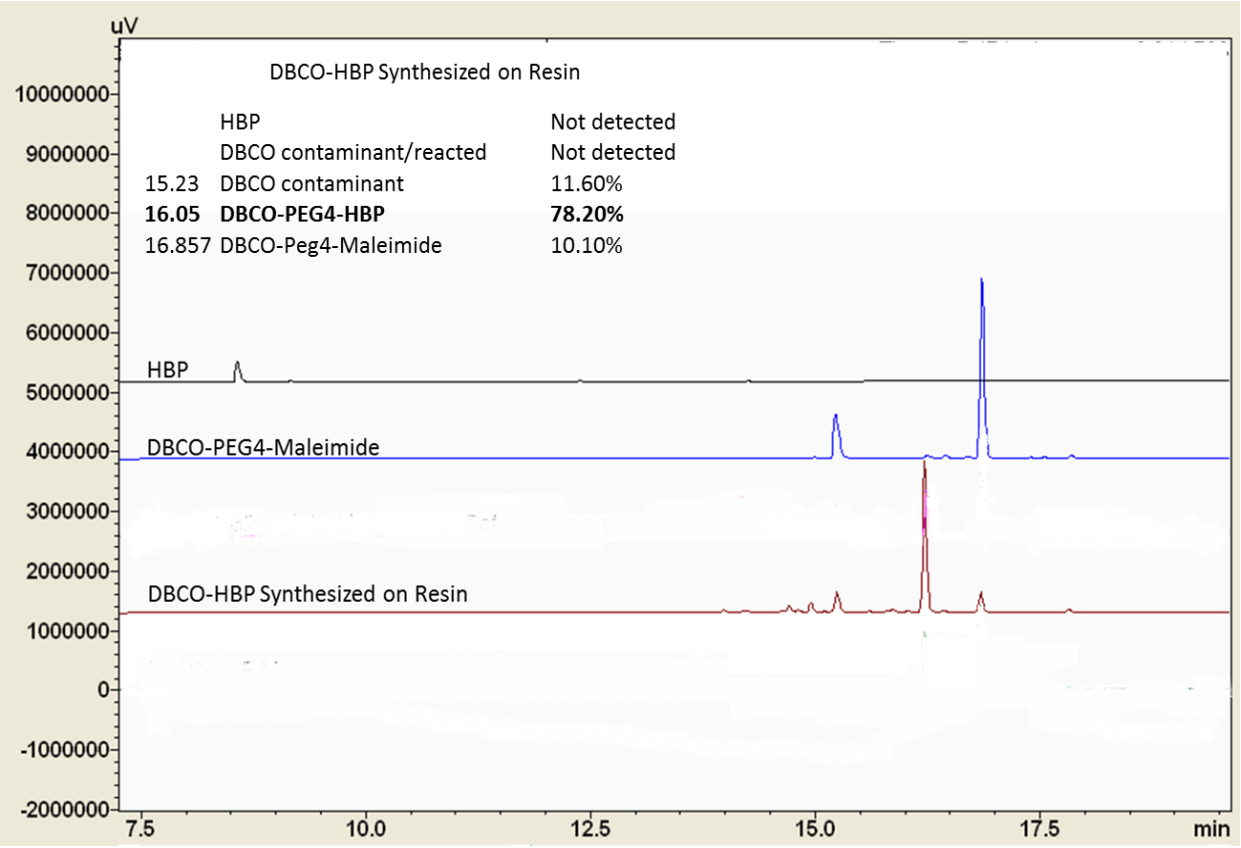

Figure 4: High performance liquid chromatography (HPLC) quantification of DBCO-HBP conjugates.

3.2 DBCO Peptide Surface Conjugation and XPS Characterization

To assess whether DBCO-peptides were conjugated onto micropatterned PEGMA-azide brushes under copper-free click reactions, X-ray photoelectron spectroscopy (XPS) was used to confirm

peptides are covalently attached onto the R-μCP substrates. XPS is commonly used to characterize surface conjugation of small molecules as well as peptides [40]. XPS can quantitatively measure elemental composition based on binding energy. For our purpose, nitrogen is a good elemental marker to monitor before and after peptide conjugation onto R-μCP substrates. Upon binding of DBCO-peptide conjugates, the nitrogen N (1s) peak emerges at 401 eV [41]. The N (1s) peak has contributions from the amino acids and the nitrogen atoms from arginine side chains. DBCO-PEG4-RGD and DBCO-PEG4-HBP contain 16 and 22 nitrogen atoms respectively that contribute to emergence of the nitrogen peak. As experimental controls, azide functionalized R-μCP substrates not reacted with DBCO-PEG4-peptide conjugates were also analyzed using XPS (Figure 5A). Azide groups, which are highly packed on the surface, can show as a double peak at 401 eV and 405 eV as a result of the resonance that exist inherently in their structure. However, the N (1s) peak was not detected in our XPS survey when R-μCP substrates were not conjugated with a DBCO-peptide. The absence of a double azide peaks could also be from low concentration of azide groups available on surface. However, the N (1s) peak is clearly detectable for both DBCO-RGD and DBCO-HBP after conjugation of DBCO-peptides on R-μCP substrates (Figure 5B & C).

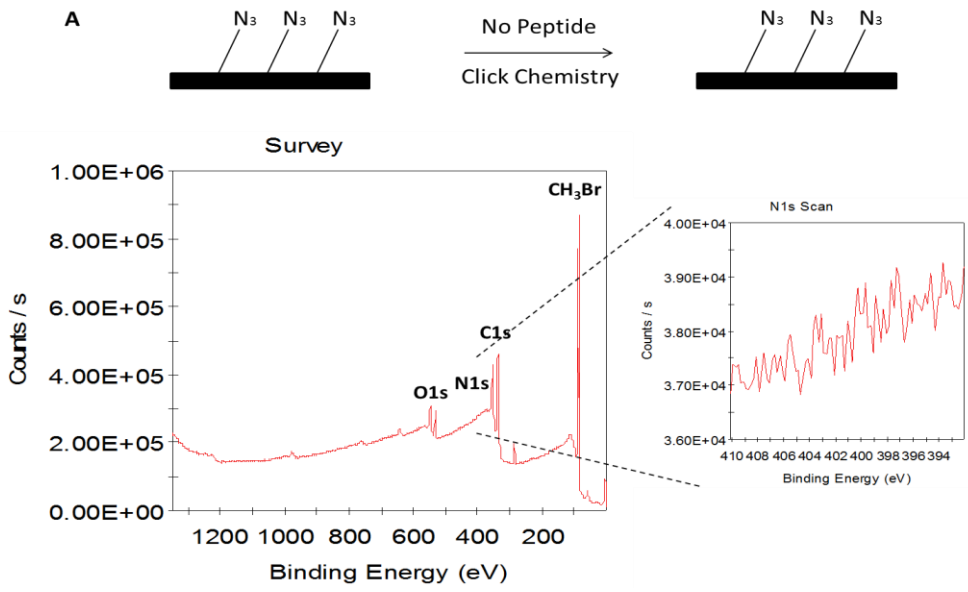

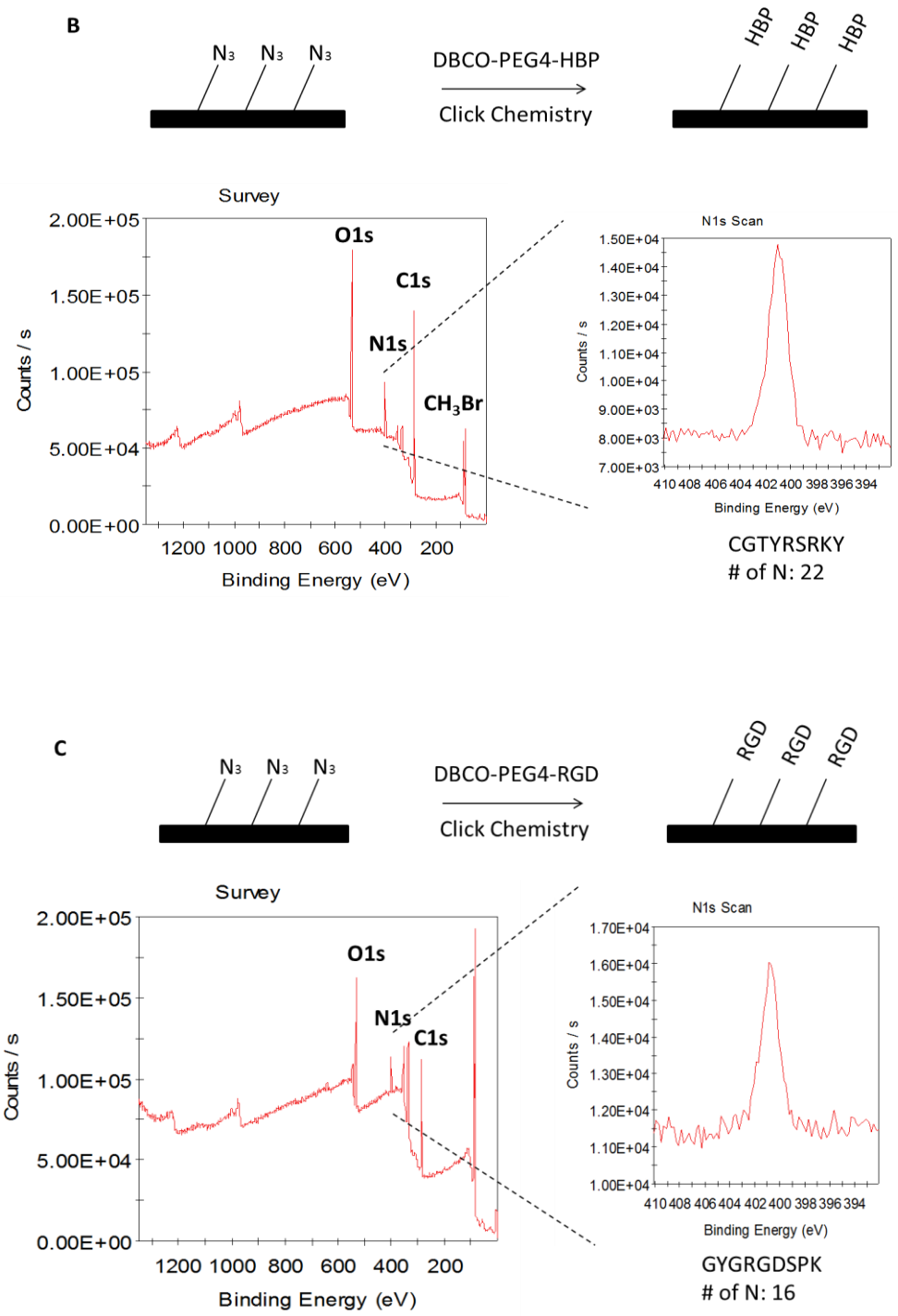

Figure 5: A) XPS characterization of azide functionalized substrates with no peptide conjugation. B) XPS characterization of azide functionalized substrates with HBP conjugation. C) XPS characterization of azide functionalized substrates with RGD peptide conjugation.

3.3 Radial Expansion of Neural Tissues by DBCO-Peptide Conjugates

After seeding hPSCs on R-μCP substrates and generation of arrays of single neural rosettes, R-μCP substrates were functionalized with DBCO-RGD and DBCO-HBP conjugates on Day 3 at 1μM, 5μM, 10μM, 15μM concentrations. After media change, the peptide conjugates were readily immobilized onto the azide functionalized PEGMA brushes. No tissue expansion was observed on DBCO-HBP conjugated substrates on Day 4 or 7 at any concentration (Figure 6).

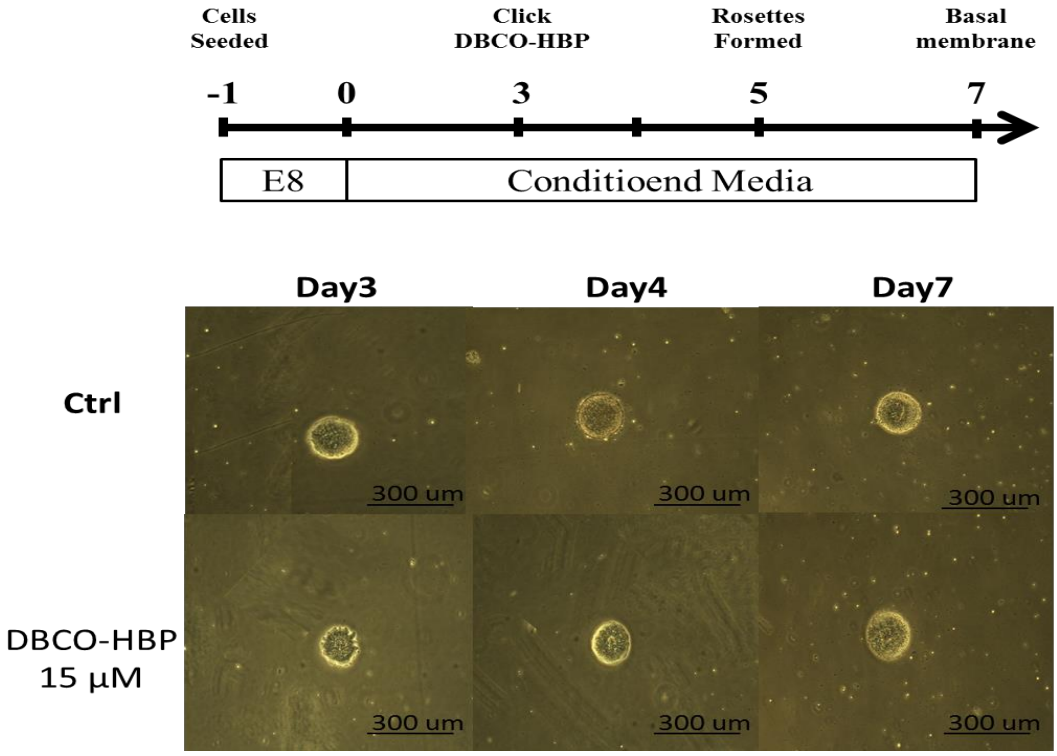

Figure 6: A) Schematic for derivation and HBP-DBCO mediated expansion of forebrain neuroepithelial tissues on R-μCP outgrowth substrates. 250μm diameter circles with 300μm outgrowth regions. No NSCs radial outgrowth after adding HBP-DBCO at Day 3.

Upon conjugation of DBCO-RGD 15μM on R-μCP substrates a gradual expansion of neural tissues was observed on R-μCP substrates. Brightfield images of 20x magnification were taken and tissue outgrowth was quantified and 85% of neural tissues were fully expanded on Day 7 (Figure 7).

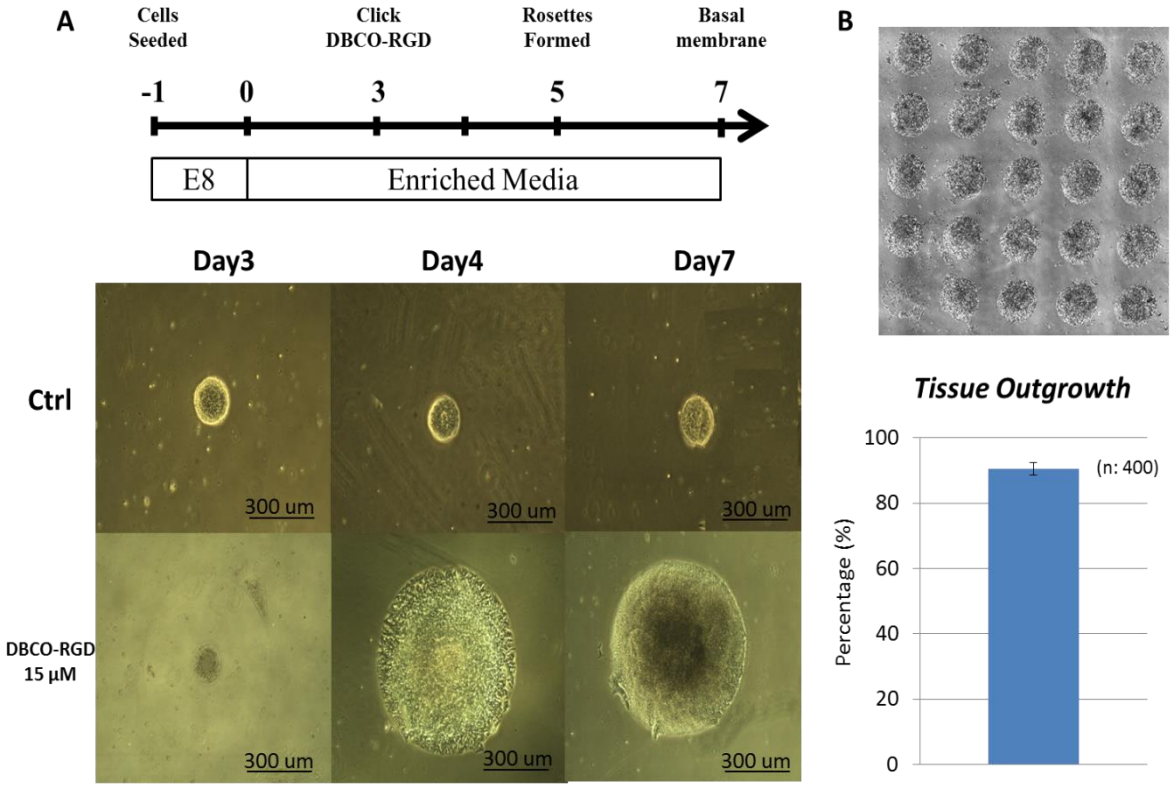

Figure 7: A) Schematic for derivation and RGD-DBCO mediated expansion of forebrain neuroepithelial tissues on R-μCP outgrowth substrates. 250 μm diameter circles with 300 μm outgrowth regions. NSCs radial outgrowth after adding RGD-DBCO 15 μM at Day 3. B) NSCs tissue outgrowth on R-μCP outgrowth substrates at Day 7. Four biological replicates (# of slides) were assayed to reach n=400.

R-μCP substrates conjugated with 1 μM, 5μM, 10μM, 15μM of DBCO-RGD demonstrated different rates of tissue outgrowth from images captured by brightfield microscopy. This indicates a direct correlation between DBCO-RGD surface density and tissue expansion on R-μCP substrates (Figure 8).

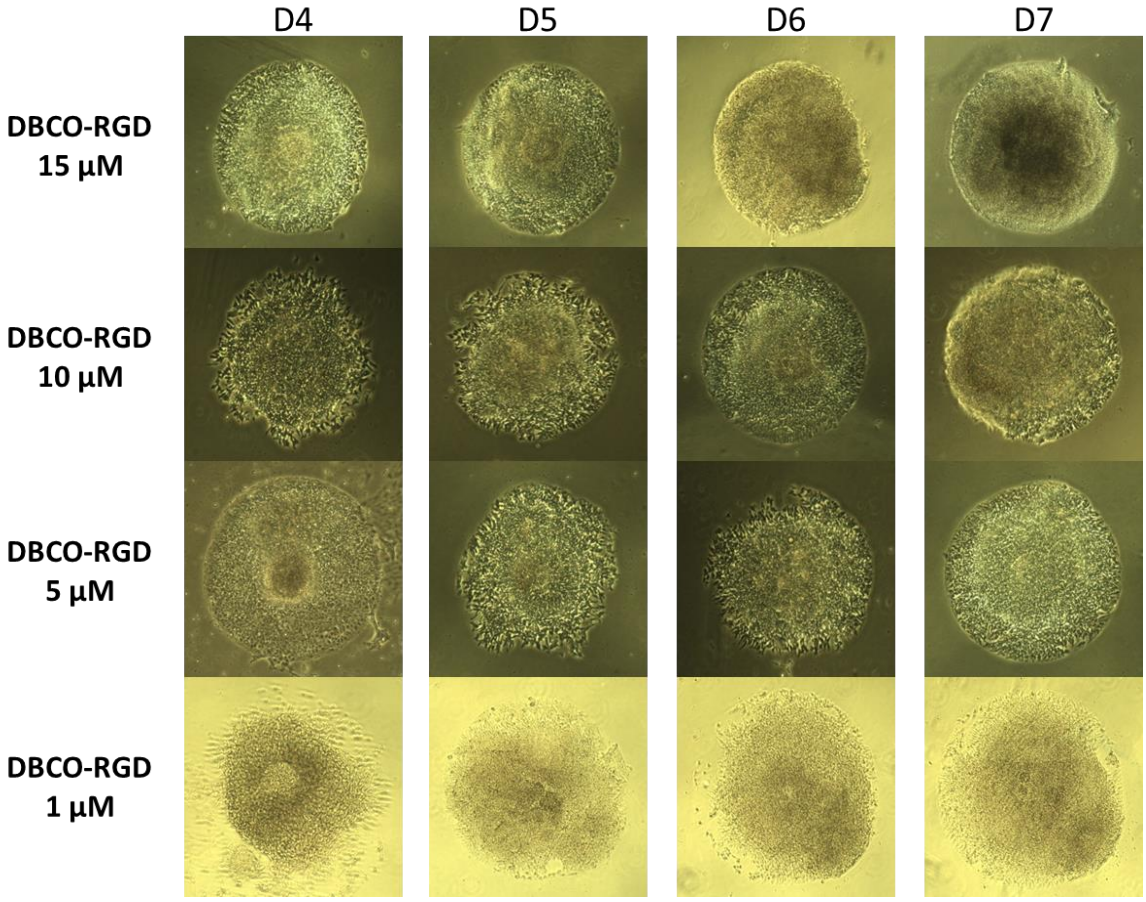

Figure 8: RGD-DBCO mediated expansion of forebrain neuroepithelial tissues on R-μCP outgrowth substrates at different concentrations added on day 3 and radial NSCs expansion at different days. The micropatterned outgrowth annulus is 250 μm ID with a 300 μm OD.

Immunostaining of expanded tissues on Day 7 revealed a correlation between the number of resulting neural rosette polarizations and DBCO-RGD concentration (Figure 9). We quantified the amount of neural rosettes formation at different DBCO-RGD concentrations. Tissue expansion with 15µM DBCO-RGD yielded 9 ± 2 rosettes on Day 7 of outgrowth. The amount of neural rosettes formation on Day 7 dropped with a decrease in DBCO-RGD concentration to 5 ± 2 and 2 ± 1 rosettes at 10µM and 5µM DBCO-RGD concentrations, respectively (Figure 10).

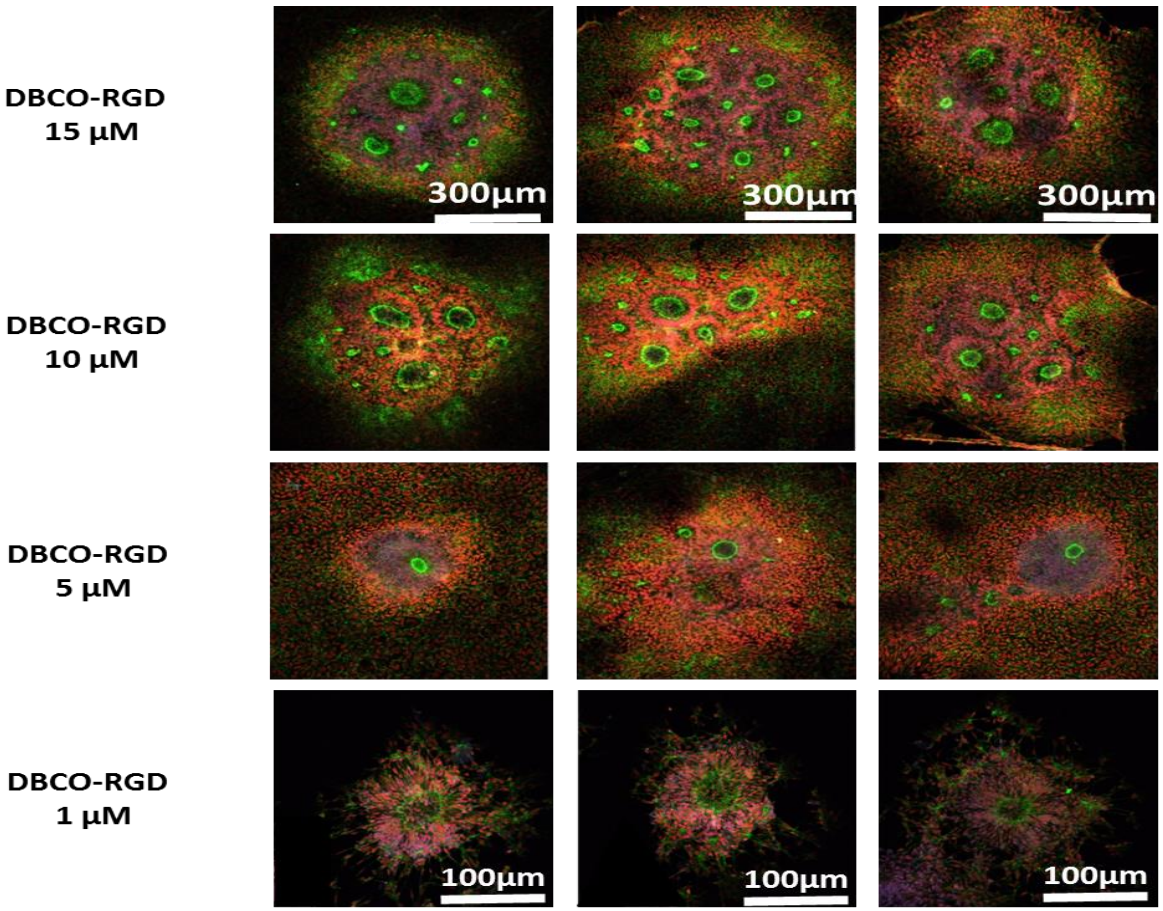

Figure 9: Immunostaining for N-cadherin (green) and Pax6 (red) upon NSCs radial outgrowth on day 7 after adding RGD-DBCO at different concentrations on day3. 250µm diameter circles with 300µm outgrowth regions.

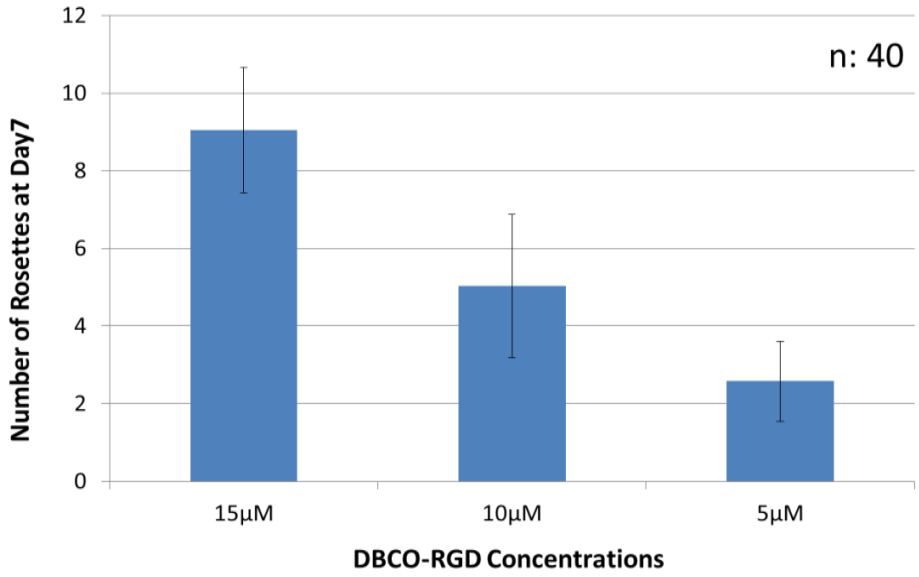

Figure 2: Manual quantification of polarization foci/neural rosettes per tissue at different DBCO-RGD concentrations on Day 7 with the number of tissues (technical replicates) analyzed per condition indicated above the bar.

4. Conclusion and Final Remarks

Using clickable peptide conjugates can convert azide functionalized PEGMA brushes into biospecific and cell-adhesive surface that can permit radial tissue growth. DBCO-RGD peptide, a biomimetic fibronectin peptide, demonstrated in situ conversion of azide functionalized PEGMA, which initially confined hPSC-derived neural tissues to a microscale circular morphology. This progression in tissue morphology can potentially mimic early developments in morphogenesis of central nervous system and generate arrays of neuroepithelial tissues with cytoarchitecture analogous to developing neural tube slice cultures. This methodology for controlled spatiotemporal changes in the morphology of 2D hPSC-derived single neural rosettes tissues can be widely applicable for establishment of multiple organized populations of neuronal cell types and maintenance of a polarized population of NSCs without further substrate modifications.

In human corticogenesis, asymmetric division of ventricular zone, telencephalic neuroepithelial cells (NECs) generate a consistent cohort of neuronal and glial cell phenotypes in a stereotyped temporal manner. This developmental process can be recapitulated in vitro in 3-D cerebral organoid cultures [42]. However, in 3-D culture platforms, neuroepithelial tissues, a.k.a. neural rosettes, form spontaneously with arbitrary shape, size, and number. Since each neural rosette can act as an independent foci of cerebral morphogenesis, this can impede standardization of in vitro corticogenesis within these platforms using current methods [43, 44]. Our novel microarray culture platform induces consistent formation of hPSC-derived telencephalic neural tissues with uniform shape and size and comprised of a singular neural rosette, potentially enabling standardization of their subsequent corticogenesis [45-47].

Our preliminary experiments allowed radial migration of NSCs away from micropatterned neural rosette resulted in neuronal differentiation and partial breakdown of polarity. We expect that combining the innate spontaneous morphogenetic potential of stem cells elegantly demonstrated in 3D cerebral organoid protocols, with the macroscale morphological control demonstrated in 2D microcontact printed platforms presented here could provide the first example of highly reproducible and developmentally biomimetic formation of cerebral tissue analogs. We hope to eventually demonstrate reproducible formation of arrays of cerebral slice culture organoids with macroscale biomimicry of in vivo corticogenesis (Figure 11).

The platform developed here enables controlled radial expansion of single rosettes and can be further combined with region-specific NSC derivation protocols to enable biomanufacture of organotypic human CNS tissue slices. Interfacing this platform with techniques for hPSC gene-editing and patient-specific cellular reprogramming could allow for advanced study of neurodegenerative disease mechanisms and open the door for potentially novel high throughput

drug and toxin screening methods. Ultimately, the work presented here will lay the foundation for facilitating a greater understanding of neurodegenerative disease prevention and treatment.

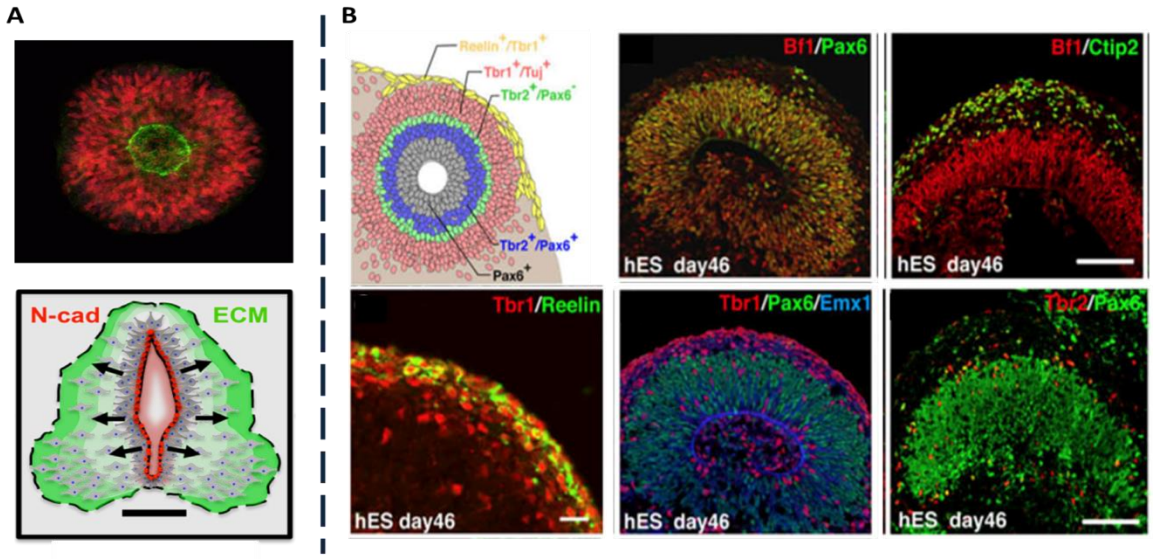

Figure 11: A) Representative immunostained images of single rosettes with a layer of columnar pax6 positive neuroepithelial cells (red) exhibiting apical polarization of N-cadherin (green) and a schematic of their radial expansion. B) Forebrain development into the classic stratified cerebral cortical structure [15].

Appendix 1: Streptavidin Surface Density Standard Curve

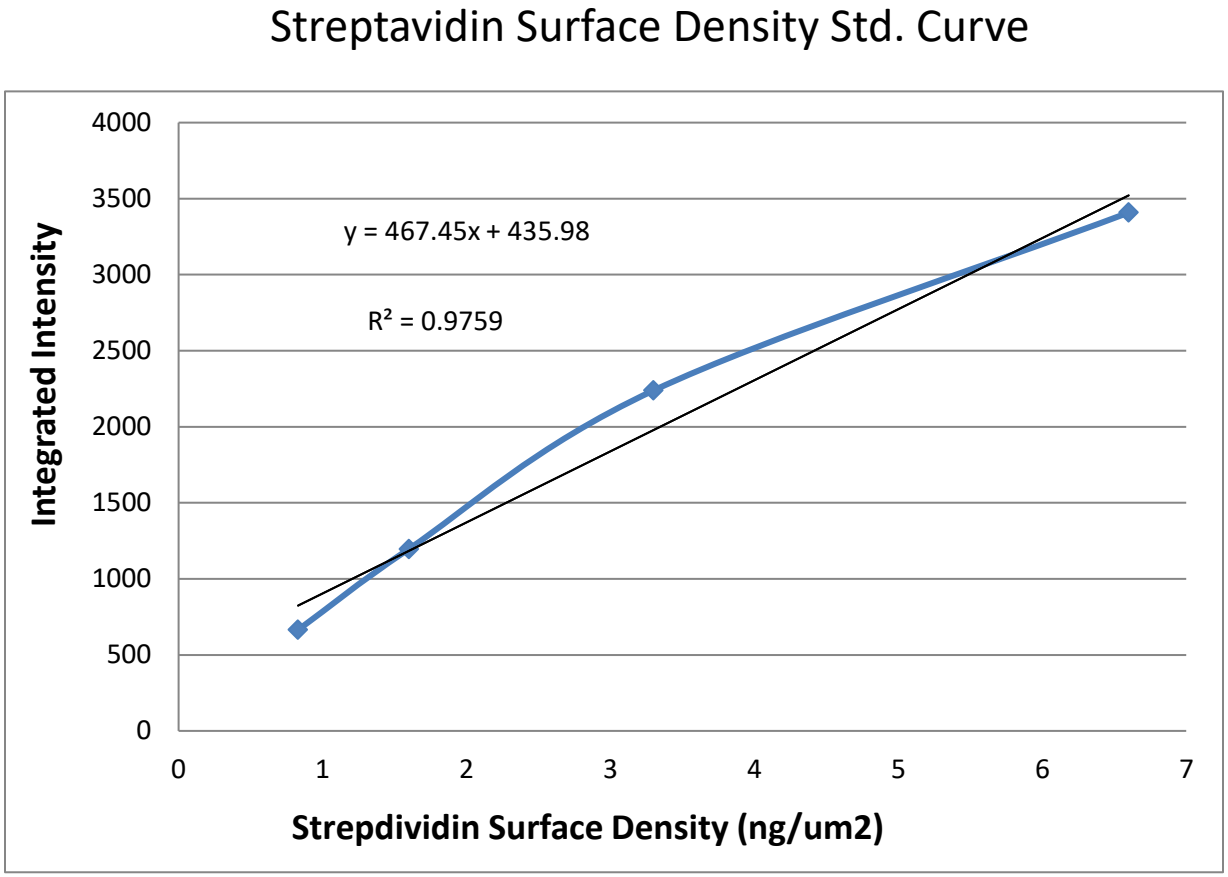

Figure 1: Standard curve equation derived to correlate fluorescent intensity of the patterns to the Streptavidin-546 surface density (ng/μm^2).

Appendix 2: Offset Calculations for Robotic Microcontact patterned Substrates

Initial Conditions

```
close all;
clear all;
file='large image 3 post (11-29).txt';
dataP1=load(file);
file1='large image 3 well (11-29).txt';
dataW1=load(file1);
conversion = 0.4029; %pixels/um
Postx_coord1=dataP1(:,6);%./conversion;
Posty_coord1=dataP1(:,7);%./conversion;
Wellx_coord1=dataW1(:,6);%./conversion;
Welly_coord1=dataW1(:,7);%./conversion;
```

Translation of Matrix

```
x_trans = Postx_coord1(1)-Wellx_coord1(1);
y_trans = Posty_coord1(1)-Welly_coord1(1);
Wellx_coordT=Wellx_coord1+x_trans;
Welly_coordT=Welly_coord1+y_trans;
Wellaveragex=mean(Wellx_coord1);
Wellaveragey=mean(Welly_coord1);
Postaveragex=mean(Postx_coord1);
Postaveragey=mean(Posty_coord1); CWell=[Wellaveragex+x_trans,Wellaveragey+y_trans];
```

```
CPost=[Postaveragex,Postaveragey]
```

Angular Offset Calculation

```
x=[0:1];
Wellfit=(CWell(2)-Posty_coord1(1))*x+Posty_coord1(1);
Postfit=(CPost(2)-Posty_coord1(1))*x+Posty_coord1(1);
%CWellvec=[Postx_coord1(1) CWell(2)];
%Postvec=[Postx_coord1(1) CPost(2)];
CWellvec=[(CWell(1)-Postx_coord1(1)) (CWell(2)-Posty_coord1(1))];
Postvec=[(CPost(1)-Postx_coord1(1)) (CPost(2)-Posty_coord1(1))];
CWellmag=norm(CWellvec);
CPostmag=norm(Postvec);
dotprod=dot(CWellvec,Postvec);
Angular_offset= acos(dotprod/(CWellmag*CPostmag));
Degrees = radtodeg(Angular_offset);
disp(['The angular offset is ',num2str(Degrees),' degrees!'])
```

The angular offset is 0.65337 degrees!

Rotation procedure

```
theta = -Degrees; % + to rotate counterclockwise, - for clockwise
R = [cosd(theta) -sind(theta); sind(theta) cosd(theta)];
P = [Postx_coord1 Posty_coord1]'; % Rotate your point(s)
W = [Wellx_coord1 Welly_coord1]'; % Rotate your point(s)
```

```
rotPost = R*P;

rotWell = R*W;

RotatedPx = rotPost(1,:)';

RotatedPy = rotPost(2,:)';

RotatedWx = rotWell(1,:)';

RotatedWy = rotWell(2,:)';

W_C = [Wellaveragex, Wellaveragey]';

rotWell_C = R*W_C;

RotatedW_C=rotWell_C';

WellfitR=(RotatedW_C(2)-Welly_coord1(1))*x+Welly_coord1(1);

W_T = [Wellx_coordT Welly_coordT]';

rotWell_T = R*W_T;

RotatedWx_T = rotWell_T(1,:)';

RotatedWy_T = rotWell_T(2,:)';

CW_T = [CWell(1) CWell(2)]';

rotCW_T = R*CW_T;

RotatedCW_T = rotCW_T';

WellfitRT=(RotatedCW_T(2)-Posty_coord1(1))*x+Posty_coord1(1);
```

Plot Unaltered Data

```
figure(1);

hold on
```

```
%Plot Well grid
plot([Wellx_coord1(1) Wellx_coord1(2)],[Welly_coord1(1)
Welly_coord1(2)],'g-o')
plot([Wellx_coord1(2) Wellx_coord1(3)],[Welly_coord1(2)
Welly_coord1(3)],'g-o')
plot([Wellx_coord1(3) Wellx_coord1(4)],[Welly_coord1(3)
Welly_coord1(4)],'g-o')
plot([Wellx_coord1(4) Wellx_coord1(1)],[Welly_coord1(4)
Welly_coord1(1)],'g-o')
%Plot Well Centroid
plot(Wellaveragex, Wellaveragey,'g*');
%Plot Post grid
plot([Postx_coord1(1) Postx_coord1(2)],[Posty_coord1(1)
Posty_coord1(2)],'r-o')
plot([Postx_coord1(2) Postx_coord1(3)],[Posty_coord1(2)
Posty_coord1(3)],'r-o')
plot([Postx_coord1(3) Postx_coord1(4)],[Posty_coord1(3)
Posty_coord1(4)],'r-o')
plot([Postx_coord1(4) Postx_coord1(1)],[Posty_coord1(4)
Posty_coord1(1)],'r-o')
%Plot Post Centroid
plot(Postaveragex,Postaveragey,'r*')
title('Post and Well Overlay')
```

```
xlabel('X dimension (um)')
ylabel('Y dimension (um)')
```

Results after Rotation

```
%Calculate Horizontal Offset
point1H=abs(RotatedWx(1)-Postx_coord1(1))
point2H=abs(RotatedWx(2)-Postx_coord1(2))
point3H=abs(RotatedWx(3)-Postx_coord1(3))
point4H=abs(RotatedWx(4)-Postx_coord1(4))
%point1H=abs(Wellx_coord1(1)-Postx_coord1(1))
%point2H=abs(Wellx_coord1(2)-Postx_coord1(2))
%point3H=abs(Wellx_coord1(3)-Postx_coord1(3))
%point4H=abs(Wellx_coord1(4)-Postx_coord1(4))
Percent_1H=(point1H/800)*100
Percent_2H=(point2H/800)*100
Percent_3H=(point3H/800)*100
Percent_4H=(point4H/800)*100
HorizOffset=[point1H;point2H;point3H;point4H];
Percent_H_Offset=[Percent_1H;Percent_2H;Percent_3H;Percent_4H];
```

```
Average_Horizontal_Offset=mean(HorizOffset) %um

Percent_Horizontal_Offset=mean(Percent_H_Offset) %percent

%Calculate Vertical Offset

point1V=abs(RotatedWy(1)-Posty_coord1(1))

point2V=abs(RotatedWy(2)-Posty_coord1(2))

point3V=abs(RotatedWy(3)-Posty_coord1(3))

point4V=abs(RotatedWy(4)-Posty_coord1(4))

%point1V=abs(Welly_coord1(1)-Posty_coord1(1))

%point2V=abs(Welly_coord1(2)-Posty_coord1(2))

%point3V=abs(Welly_coord1(3)-Posty_coord1(3))

%point4V=abs(Welly_coord1(4)-Posty_coord1(4))

Percent_1V=(point1V/1200)*100

Percent_2V=(point2V/1200)*100

Percent_3V=(point3V/1200)*100

Percent_4V=(point4V/1200)*100

VertOffset=[point1V;point2V;point3V;point4V];

Percent_V_Offset=[Percent_1V;Percent_2V;Percent_3V;Percent_4V];
```

Average_Vertical_Offset=mean(VertOffset) %um

Percent_Vertical_Offset=mean(Percent_V_Offset) %percent

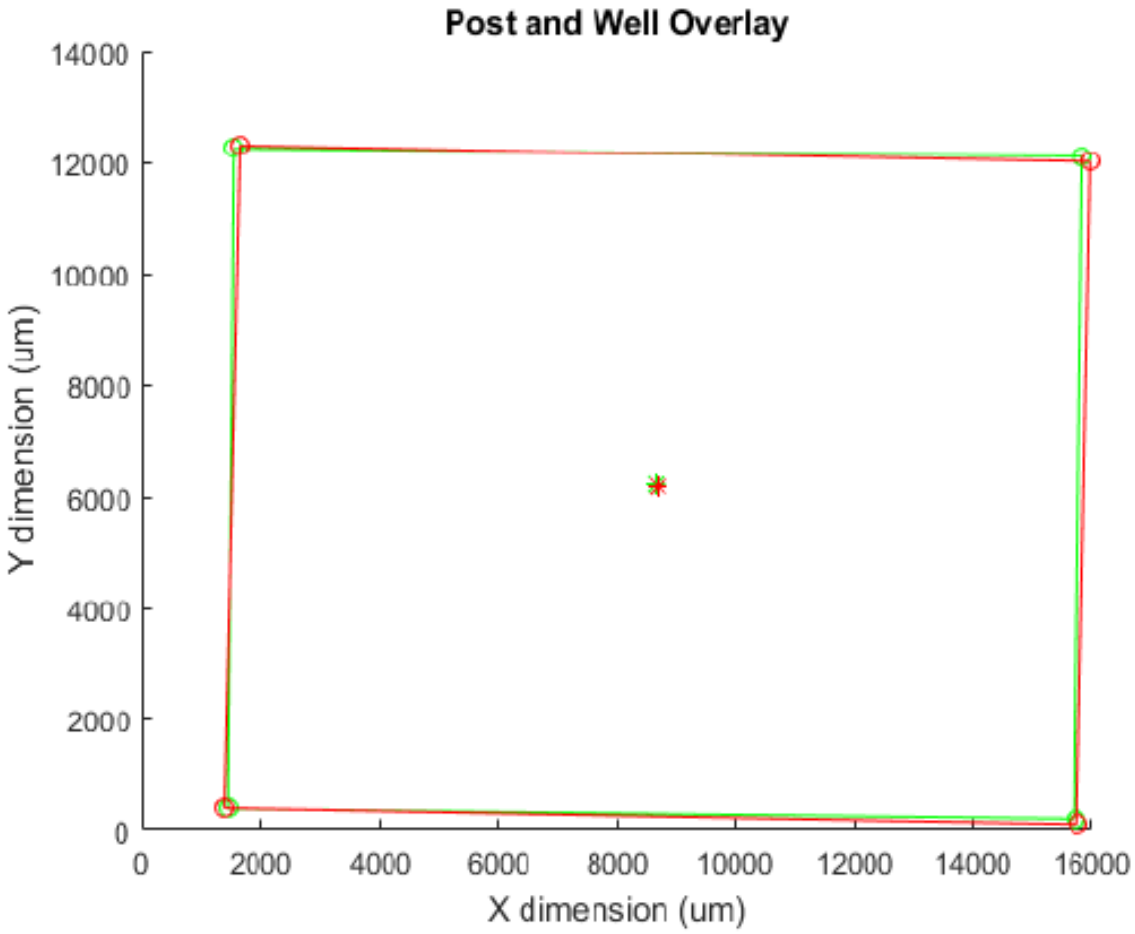

Translate Well Matrix and Plot

```
figure(2);
hold on
%Plot Translated Well Grid
plot([Wellx_coord1(1)+x_trans Wellx_coord1(2)+x_trans],
[Welly_coord1(1)+y_trans Welly_coord1(2)+y_trans],'g-o')
plot([Wellx_coord1(2)+x_trans Wellx_coord1(3)+x_trans],
[Welly_coord1(2)+y_trans Welly_coord1(3)+y_trans],'g-o')
plot([Wellx_coord1(3)+x_trans Wellx_coord1(4)+x_trans],
[Welly_coord1(3)+y_trans Welly_coord1(4)+y_trans],'g-o')
plot([Wellx_coord1(4)+x_trans Wellx_coord1(1)+x_trans],
[Welly_coord1(4)+y_trans Welly_coord1(1)+y_trans],'g-o')
%Plot Translated Well Centroid
plot(CWell(1),CWell(2),'g*');
%Plot line from centroid to point
plot([Postx_coord1(1) CWell(1)],Wellfit,'g');
%Plot Post grid
```

```
plot([Postx_coord1(1) Postx_coord1(2)],[Posty_coord1(1)
Posty_coord1(2)],'r-o')
plot([Postx_coord1(2) Postx_coord1(3)],[Posty_coord1(2)
Posty_coord1(3)],'r-o')
plot([Postx_coord1(3) Postx_coord1(4)],[Posty_coord1(3)
Posty_coord1(4)],'r-o')
plot([Postx_coord1(4) Postx_coord1(1)],[Posty_coord1(4)
Posty_coord1(1)],'r-o')
%Plot Post Centroid
plot(CPost(1),CPost(2),'r*');
%Plot line from centroid to point
plot([Postx_coord1(1) CPost(1)],Postfit,'r');
title('Post and Translated Well Overlay')
xlabel('X dimension (um)')
ylabel('Y dimension (um)')
%axis([0 13000 0 14000])
```

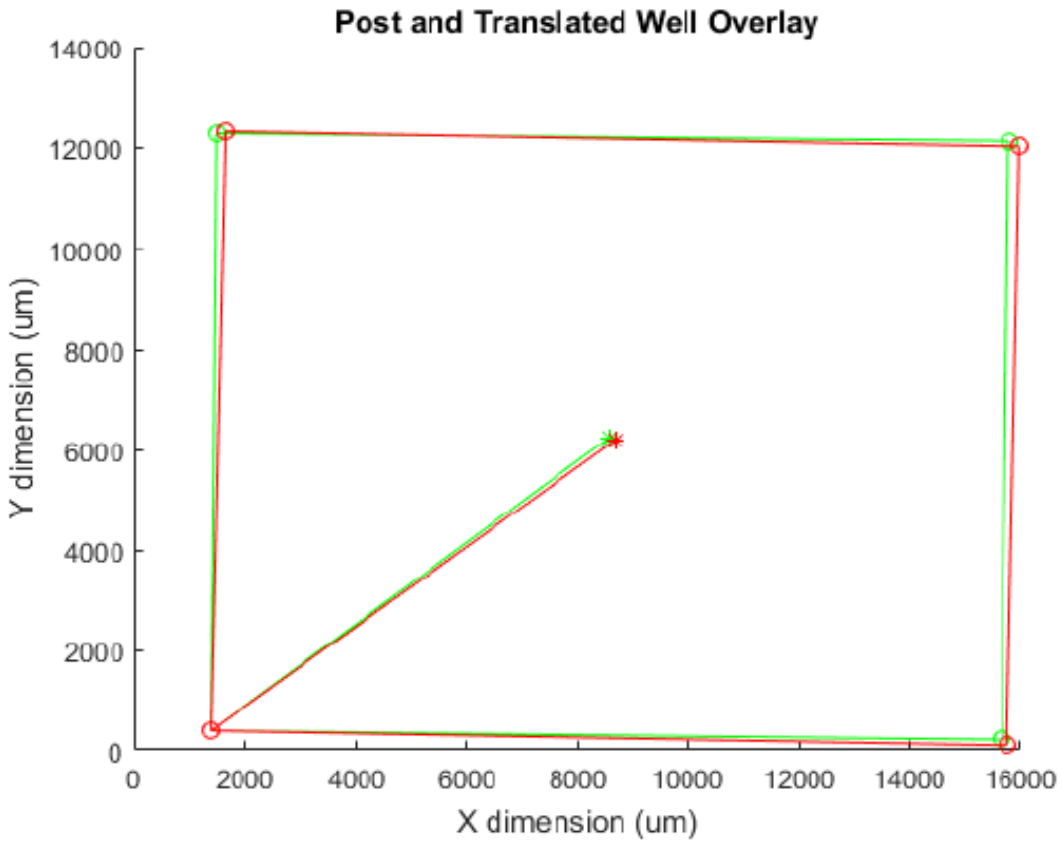

Rotate Translated Well

```
figure(3);
hold on
%Plot Roatated Translated Well Grid
plot([RotatedWx_T(1) RotatedWx_T(2)],[RotatedWy_T(1)
RotatedWy_T(2)], 'g-o')
plot([RotatedWx_T(2) RotatedWx_T(3)],[RotatedWy_T(2)
RotatedWy_T(3)], 'g-o')
plot([RotatedWx_T(3) RotatedWx_T(4)],[RotatedWy_T(3)
RotatedWy_T(4)], 'g-o')
```

```
plot([RotatedWx_T(4) RotatedWx_T(1)],[RotatedWy_T(4)
RotatedWy_T(1)], 'g-o')
%Plot Rotated Translated Well Centroid
plot(RotatedCW_T(1),RotatedCW_T(2),'g*');

%Plot line from centroid to point
plot([Postx_coord1(1) RotatedCW_T(1)],WellfitRT,'g');
%Plot Post grid
plot([Postx_coord1(1) Postx_coord1(2)],[Posty_coord1(1)
Posty_coord1(2)],'r-o')
plot([Postx_coord1(2) Postx_coord1(3)],[Posty_coord1(2)
Posty_coord1(3)],'r-o')
plot([Postx_coord1(3) Postx_coord1(4)],[Posty_coord1(3)
Posty_coord1(4)],'r-o')
plot([Postx_coord1(4) Postx_coord1(1)],[Posty_coord1(4)
Posty_coord1(1)],'r-o')
%Plot Post Centroid
plot(CPost(1),CPost(2),'r*');
%Plot line from centroid to point
plot([Postx_coord1(1) CPost(1)],Postfit,'r');
title('Post and Rotated Translated Well Overlay')
xlabel('X dimension (um)')
ylabel('Y dimension (um)')
```

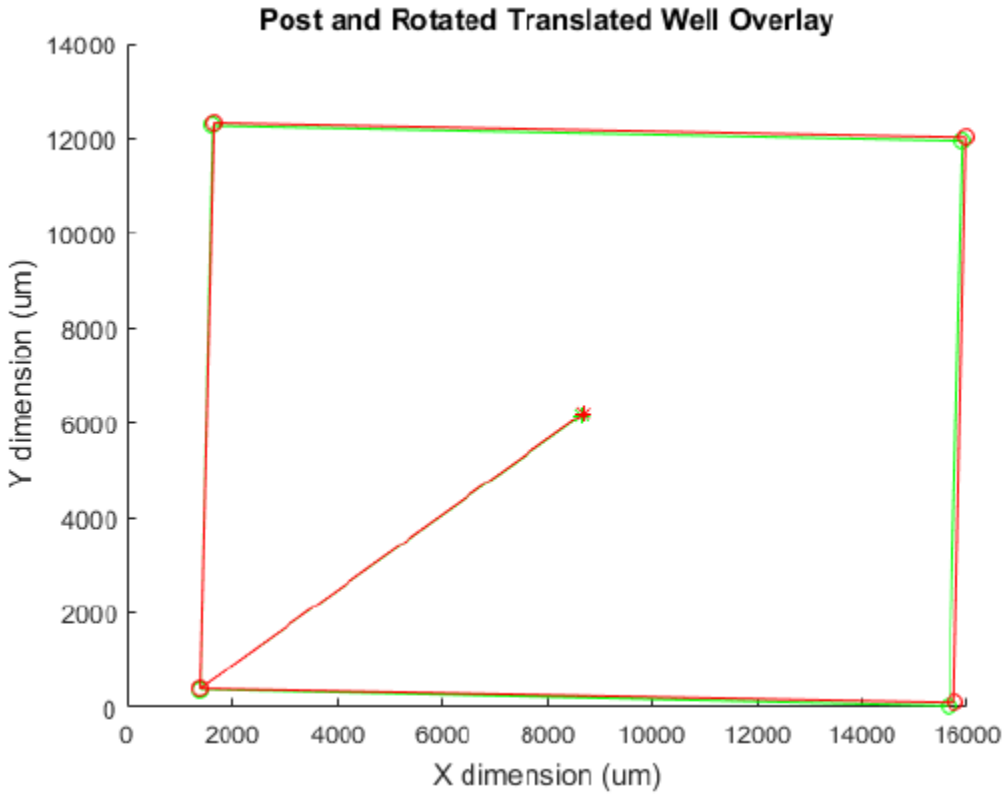

Plot Original Matrices (Rotated Well)

```
figure(4);
hold on
%Plot Rotated Well Grid
plot([RotatedWx(1) RotatedWx(2)],[RotatedWy(1) RotatedWy(2)], 'g-o')

plot([RotatedWx(2) RotatedWx(3)],[RotatedWy(2) RotatedWy(3)], 'g-o')
plot([RotatedWx(3) RotatedWx(4)],[RotatedWy(3) RotatedWy(4)], 'g-o')
plot([RotatedWx(4) RotatedWx(1)],[RotatedWy(4) RotatedWy(1)], 'g-o')
%Plot Rotated Well Centroid
plot(RotatedW_C(1),RotatedW_C(2),'g*')
%Plot line from centroid to point
```

```
%plot([RotatedWx(1) RotatedW_C(1)],WellfitR,'g');
%Plot Post grid
plot([Postx_coord1(1) Postx_coord1(2)],[Posty_coord1(1)
Posty_coord1(2)],'r-o')
plot([Postx_coord1(2) Postx_coord1(3)],[Posty_coord1(2)
Posty_coord1(3)],'r-o')
plot([Postx_coord1(3) Postx_coord1(4)],[Posty_coord1(3)
Posty_coord1(4)],'r-o')
plot([Postx_coord1(4) Postx_coord1(1)],[Posty_coord1(4)
Posty_coord1(1)],'r-o')
%Plot Post Centroid
plot(CPost(1),CPost(2),'r*');
%Plot line from centroid to point
%plot([Postx_coord1(1) CPost(1)],Postfit,'r');
title('Post and Rotated Well Overlay')
xlabel('X dimension (um)')
ylabel('Y dimension (um)')
```

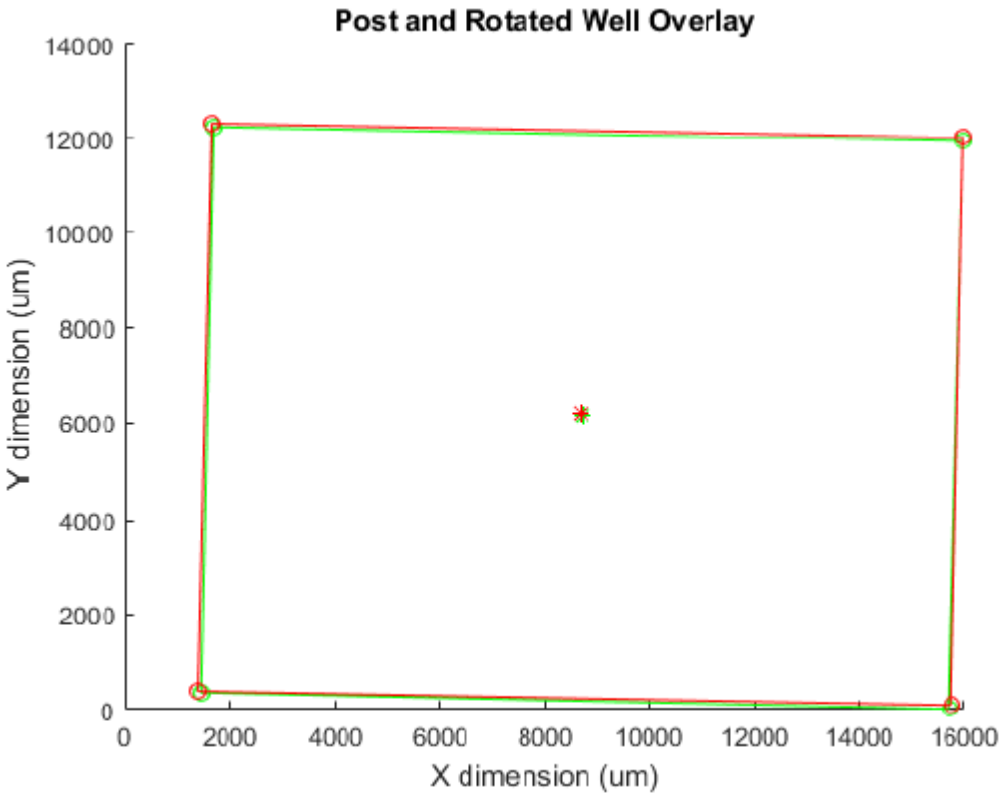
Post and Rotated Well Overlay
Y dimension (um)
X dimension (um)
0
2000
4000
6000
8000
10000
12000
14000
16000

References

1. Malcolm R. Alison1, Richard Poulsom, Stuart Forbes and Nicholas A. Wright. (2002) An introduction to stem cells. Journal of Pathology 197: 419–423.
2. Allan Spradling, Daniela Drummond-Barbosa & Toshie Kai. (2001) Stem cells find their niche. Nature Vol 414.
3. Wojciech Zakrzewski, Maciej Dobrzyński, Maria Szymonowicz and Zbigniew Rybak. (2019) Stem cells: past, present, and future. Stem Cell Research & Therapy 10:68.
4. In-Hyun Park, Paul H Lerou, Rui Zhao, Hongguang Huo and George Q Daley. (2008) Generation of human-induced pluripotent stem cells. Nature Protocols Vol.3 NO.7.
5. Lindvall O, Brundin P, Widner H, Rehncrona S, Gustavii B, Frackowiak R, Leenders KL, Sawle G, Rothwell JC, Marsden CD: Grafts of fetal dopamine neurons survive and improve motor function in Parkinson's disease. Science 1990, 247:574-577.
6. Lippmann ES, Estevez-Silva MC, Ashton RS: Defined human pluripotent stem cell culture enables highly efficient neuroepithelium derivation without small molecule inhibitors. Stem Cells 2014, 32:1032-1042.
7. Chambers SM, Fasano CA, Papapetrou EP, Tomishima M, Sadelain M, Studer L: Highly efficient neural conversion of human ES and iPS cells by dual inhibition of SMAD signaling. Nat. Biotechnol. 2009, 27:275-280.
8. Li XJ, Zhang X, Johnson MA, Wang ZB, LaVaute T, Zhang SC: Coordination of sonic hedgehog and Wnt signaling determines ventral and dorsal telencephalic neuron types from human embryonic stem cells. Development 2009, 136:4055-4063.

9. Kristen A Lemke, Alireza Aghayee, Randolph Ashton. (2017) Deriving, regenerating, and engineering CNS tissues using human pluripotent stem cells, Current Opinion in Biotechnology 2017, 47:36–42.
10. Scott F Gilbert. (2000) Developmental Biology, 6th edition.
11. Sadler, T. (2005) Embryology of neural tube development. Am. J. Med. Genet. 135C, 2–8.
12. Dady, A., Blavet, C. & Duband, J.-L. (2012) Timing and kinetics of E- to N-cadherin switch during neurulation in the avian embryo. Dev. Dyn. 241, 1333–1349.
13. Carlos R. Marti-Figueroa, Randolph S. Ashton. (2017) The case for applying tissue engineering methodologies to instruct human organoid morphogenesis. Acta Biomaterialia 54 35–44.
14. Sun, T. & Hevner, R. F. (2014) Growth and folding of the mammalian cerebral cortex: from molecules to malformations. Nat Rev Neurosci 15, 217–232.
15. Eiraku M, et al. (2008) Self-organized formation of polarized cortical tissues from ESCs and its active manipulation by extrinsic signals. Cell Stem Cell 6, 3(5):519-32.
16. Haubst, N. (2006) Basement membrane attachment is dispensable for radial glial cell fate and for proliferation, but affects positioning of neuronal subtypes. Development 133, 3245 3254.
17. Pasko Rakic, (2007) The radial edifice of cortical architecture: From neuronal silhouettes to genetic engineering. Brain Res Rev. 55(2): 204–219.
18. Shen, Q. et al. (2006) The timing of cortical neurogenesis is encoded within lineages of individual progenitor cells. Nat Neurosci 9, 743–751
19. Dehay C, et al. (2007) Cell-cycle control and cortical development, Nat Rev Neurosci 8(7):568.

20. Justin T. Koepsel and William L. Murphy. (2012) Patterned Self-Assembled Monolayers: Efficient,Chemically Defined Tools for Cell Biology. ChemBioChem, 13, 1717 – 1724
21. Milan Mrksich and George M. Whitesides. (1996) Using self-assembled monolayers to understand the interactions of man-made surfaces with proteins and cells. Annu. Rev. Biophys. Biomol. Struct. 2555-78.
22. Nolan T. Flynn, Thanh Nga T. Tran, Michael J. Cima and Robert Langer. (2003) Langmuir, 19, 10909-10915.
23. Mahentha Krishnamoorthy, Shoghik Hakobyan, Madeleine Ramstedt and Julien E. Gautrot. (2014) Surface-Initiated Polymer Brushes in the Biomedical Field: Applications in Membrane Science, Biosensing, Cell Culture, Regenerative Medicine and Antibacterial Coatings. Chem. Rev. 114, 10976−11026.
24. Myungwoong Kim, Samantha K. Schmitt, Jonathan W. Choi, John D. Krutty and Padma Gopalan. (2015) From Self-Assembled Monolayers to Coatings: Advances in the Synthesis and Nanobio Applications of Polymer Brushes. Polymers 7, 1346-1378.
25. Maria Pardo-Figuerez, Neil R. W. Martin, Darren J. Player, Paul Roach, Steven D. R. Christie, Andrew J. Capel, and Mark P. Lewis. (2018) Controlled Arrangement of Neuronal Cells on Surfaces Functionalized with Micropatterned Polymer Brushes. American Chemical Society 12383−12391.
26. Younan Xia and George M. Whitesides. (1998) Soft Lithography. Annu. Rev. Mater. Sci. 1998. 28:153–84.
27. George M. Whitesides, Emanuele Ostuni, Shuichi Takayama, Xingyu Jiang, and Donald E. Ingber. (2001) SOFT LITHOGRAPHY IN BIOLOGY AND BIOCHEMISTRY. Annu. Rev. Biomed. Eng. 3:335–73.

28. Ravi S. Kane, Shuichi Takayama, Emanuele Ostun, Donald E. Ingber, George M. Whitesides. (1999) Patterning proteins and cells using soft lithography. Biomaterials 20 2363-2376.
29. Jin Sha, Ethan S. Lippmann, Jason McNulty, Yulu Ma, and Randolph S. Ashton. (2013) Sequential Nucleophilic Substitutions Permit Orthogonal Click Functionalization of Multicomponent PEG Brushes. Biomacromolecules 14, 3294−3303.
30. G. T. Knight, J. Sha, and R. S. Ashton. (2012) Micropatterned, clickable culture substrates enable in situ spatiotemporal control of human PSC-derived neural tissue morphology. ChemComm 10.1039.
31. Gavin T Knight, Brady F Lundin, Nisha Iyer, Lydia MT Ashton, William A Sethares, Rebecca M Willett, Randolph Scott Ashton. (2018) Engineering induction of singular neural rosette emergence within hPSC-derived tissues. eLife 2018;7:e37549.
32. Jason D. McNulty, Tyler Klann, Jin Sha, Max Salick,ae Gavin T. Knight, Lih-Sheng Turng and Randolph S. Ashton. (2014) High-precision robotic microcontact printing (R-μCP) utilizing a vision guided selectively compliant articulated robotic arm. Lab Chip, 14, 1923.
33. Gavin T. Knight, Tyler Klann, Jason D. McNulty, Randolph S. Ashton. (2014) Fabricating Complex Culture Substrates Using Robotic Microcontact Printing (R-μCP) and Sequential Nucleophilic Substitution. Journal of Visualized Experiments 10.3791/52186.
34. R Raballo, J Rhee, R Lyn-Cook, J F Leckman, M L Schwartz, F M Vaccarino. (2000) Basic fibroblast growth factor (Fgf2) is necessary for cell proliferation and neurogenesis in the developing cerebral cortex. The Journal of Neuroscience 20(13):5012–5023.
35. Maya E. Woodbury and Tsuneya Ikezu. (2014) Fibroblast growth factor-2 signaling in neurogenesis and neurodegeneration. J Neuroimmune Pharmacol 9(2): 92–101.

36. Methichit Wattanapanitch and et al. (2014) Dual Small-Molecule Targeting of SMAD Signaling Stimulates Human Induced Pluripotent Stem Cells toward Neural Lineages. PLOS ONE e106952.
37. Stuart M. Chambers and et al. (2009) Highly efficient neural conversion of human ES and iPS cells by dual inhibition of SMAD signaling Nat Biotechnol. 27(3): 275–280.
38. Alireza Aghayee and Randolph Ashton. (2020) Methods for Controlled Induction of Singular Rosette Cytoarchitecture Within Human Pluripotent Stem Cell-Derived Neural Multicellular Assemblies. Programmed Morphogenesis pp 193-203.
39. Elizabeth A. Aisenbrey and William L. Murphy. (2020) Synthetic alternatives to Matrigel. Nat Rev Mater. 5(7): 539–551. Biomacromolecules 17, 1040−1047
40. Samantha K. Schmitt, David J. Trebatoski, John D. Krutty, Angela W. Xie, Benjamin Rollins, William L. Murphy, and Padma Gopalan. (2016) Peptide Conjugation to a Polymer Coating via Native ChemicalLigation of Azlactones for Cell Culture.
41. Samantha K. Schmitt, William L. Murphy and Padma Gopalan. (2013) Crosslinked PEG mats for peptide immobilization and stem cell adhesion. J. Mater. Chem. B, 1, 1349.
42. Elizabeth Di Lullo and Arnold R. Kriegstein. (2017) The use of brain organoids to investigate neural development and disease. Neuroscience 10.1038.
43. Aliya Fatehullah, Si Hui Tan and Nick Barker. (2016) Organoids as an in vitro model of human development and disease. Nature Cell Biology Vol 18.
44. Brigham J. Hartley and Kristen J. Brennand (2017) Neural organoids for disease phenotyping, drug screening and developmental biology studies. Neurochemistry International 106 85-93.

45. Lancaster MA, Renner M, Martin C-A, Wenzel D, Bicknell LS, Hurles ME, Homfray T, Penninger JM, Jackson AP, Knoblich JA. (2013) Cerebral organoids model human brain development and micro cephaly. Nature 501:373-379.
46. Nasu, M. et al. (2012) Robust Formation and Maintenance of Continuous Stratified Cortical Neuroepithelium by Laminin-Containing Matrix in Mouse ES Cell Culture. PLoS ONE 7, e53024.
47. M.A. Lancaster, N.S. Corsini, T.R. Burkard, J.A. Knoblich. (2016) Guided self-organization recapitulates tissue architecture in a bioengineered brain organoid model, bioRxiv 10.1101/049346.